The Astronomical Journal, 132:1445–1463, 2006 October
© 2006. The American Astronomical Society. All rights reserved. Printed in U.S.A.

SPECTRAL IRRADIANCE CALIBRATION IN THE INFRARED. XVI. IMPROVED ACCURACY IN THE INFRARED SPECTRA OF THE SECONDARY AND TERTIARY STANDARD CALIBRATION STARS

Charles W. Engelke,[1] Stephan D. Price,[2] and Kathleen E. Kraemer[2]

Received 2005 December 16; accepted 2006 March 25

ABSTRACT

We have increased the spectral resolution and accuracy of the absolute infrared spectral flux for a subset of stellar standards created by Cohen and his collaborators in previous papers in this series. We combined the moderate-resolution ($\lambda/\Delta\lambda \sim 400$) spectroscopy obtained on infrared standard stars by the Short Wavelength Spectrometer on the *Infrared Space Observatory* with high-quality photometry that is tied to our recent absolute calibration from the *Midcourse Space Experiment*. New spectra were created for 33 stars, 9 of which are Cohen et al. secondary standards and another 20 of which are tertiary standards for which Cohen adopted spectral templates. The effective temperatures and angular diameters for the stars are derived from the absolute spectra and compare favorably with independent measures of these quantities in the literature. The present spectra display systematic differences with those of Cohen and colleagues in that they have 4%–7% lower fluxes in the 1–4 μm spectral region. Our spectra remove the A–K star calibration bias recently noted in the calibration of the *Spitzer Space Telescope* camera.

Key words: infrared: stars — methods: analytical — techniques: spectroscopic

Online material: extended figure set, appendix

1. INTRODUCTION

High-quality space-based spectroscopy and radiometry were combined to improve the resolution and absolute flux accuracy of the infrared spectra for a subset of the standard calibration stars created by the pioneering efforts of Cohen and his collaborators. In their initial paper, Cohen et al. (1992a, Paper I)[3] defined their primary standards as Vega (α Lyr) and Sirius (α CMa). They established the zero-magnitude flux scale by extrapolating the absolute flux of Vega at 0.5556 μm, recommended by Hayes (1985), into the mid-infrared using the calculated spectral flux of a Kurucz ($T_{\rm eff} = 9400$ K) model atmosphere. Next, they adopted a Kurucz ($T_{\rm eff} = 9850$ K) model for the infrared spectral energy distribution of Sirius, which was placed on an absolute scale by direct infrared photometric reference to Vega. In a subsequent series of papers, Cohen et al. (1992b, Paper II; 1995, Paper IV; 1996b, Paper VII) created absolutely calibrated composite spectra for 10 bright secondary infrared standards by seaming together measured spectral fragments across the near- and mid-infrared, with each fragment referenced to the primary standards. Cohen et al. (1996a, Paper VI) adopted a model atmosphere for the spectrum of α^1 Cen and used it as a reference to create secondary composite spectra for two additional secondary standards in the southern hemisphere. Ultimately, Cohen et al. (1999, Paper X) populated the sky with a network of tertiary standards by representing their infrared energy distributions with "spectral templates" and scaling the result by photometry with respect to either a primary or secondary standard. The template for a given star was taken as the composite spectrum of the secondary standard with (nearly) the same spectral type.

Price et al. (2004) assessed the accuracy of the Cohen et al. calibration using the results of the extensive series of calibration experiments conducted with the *Midcourse Space Experiment* (*MSX*). *MSX* obtained a direct absolute calibration against five emissive reference spheres that were ejected from the spacecraft at different times during the mission and precisely measured the relative photometry between the Cohen et al. primary and secondary standards. To summarize their results, Price et al. found the following:

1. The *MSX* experiments confirmed the absolute infrared zero-magnitude flux scale proposed in Paper I over the 8–21 μm range of *MSX* bands A, C, D, and E. The absolute calibration against the reference spheres agreed with the Cohen et al. absolute zero-magnitude infrared fluxes to within the *MSX* measurement errors, which were less than the 1.45% uncertainty Cohen et al. ascribe to their zero-magnitude fluxes.
2. The *MSX* relative photometry between the standard stars agrees well on average with that derived from the Cohen et al. composite spectra *if* the infrared flux from Sirius is ~1% brighter than the flux Cohen et al. adopted in Paper I. The formal errors and biases of the *MSX* photometry for the standard stars, however, are much smaller than those cited by Cohen et al. (e.g., their uncertainties are as great as 10% in the center of the 4.3 μm CO_2 atmospheric band). The *MSX* photometry can therefore be used to improve the accuracy of the composites.

The low (~0.1 μm) spectral resolution of the Cohen et al. composite spectra smooths over the spectral details in the molecular absorptions in the atmospheres of the standard stars, which can introduce errors when calibrating narrow spectral bands or spectral measurements. Sensors that use very narrow spectral bands require photometric standards that have a sufficiently high spectral resolution to accurately reflect the spectral features that are present. The higher formal accuracy of the *MSX* photometry can be used to reduce these uncertainties, particularly when combined with higher resolution spectra from the European Space Agency's *Infrared Space Observatory* (*ISO*; Kessler et al. 2003) mission. Here we describe the procedures used to combine the

[1] Institute for Scientific Research, Boston College, 140 Commonwealth Avenue, Chestnut Hill, MA 02467; charles.engelke.ctr@hanscom.af.mil.

[2] Air Force Research Laboratory, VSB, 29 Randolph Road, Hanscom AFB, MA 01731; kathleen.kraemer@hanscom.af.mil, steve.price@hanscom.af.mil.

[3] We refer generally to the stellar calibration and standards developed by M. Cohen and his collaborators as "Cohen et al." Specific references have the year of publication and series designation for the first instance (e.g., 1992a, Paper I) and the series designation thereafter (e.g., Paper I).

TABLE 1
BEST SECONDARY STANDARDS

Star (1)	Spectral Type (2)	$T_{\rm eff}$ (K) (3)	θ (mas) (4)	Spectra[a] [to λ (μm)] (5)	Photometry[b] (6)
β Gem	K0 III	4850 ± 5%	8.03 ± 3%	SEW, SWS θ Cen[9], CVF δ Dra[16], A[35]	*MSX*, DIR, H, S, T, *IRAS*
α Boo	K1.5 III	4350 ± 1.5%	21.06 ± 1%	SEW[2.0], HW[2.4], S[22], A[35]	*MSX*, DIR, H, S
β UMi	K4 III	4150 ± 4%	10.00 ± 2%	S[17], A[35]	DIR, *IRAS*
α Tau	K5 III	4050 ± 2%	20.75 ± 1%	SEW[2.0], HW[2.4], S[35]	*MSX*, DIR, H, S
γ Dra	K5 III	4030 ± 2%	10.17 ± 1%	HW[2.4], S[26], A[35]	*MSX*, DIR, H, S
μ UMa	M0 III	3900 ± 4%	8.45 ± 2%	HW[2.4], S[17], A[35]	DIR, S, T
β And	M0 III	3900 ± 4%	13.65 ± 2%	SEW, S[27], A[35]	*MSX*, DIR, H, S
α Cet	M2 III	3750 ± 4%	12.94 ± 2%	SEW, S[27], A[35]	DIR, *IRAS*, S
γ Cru	M4 III	3626 ± 2%	26.37 ± 1%	S[35]	*MSX*, DIR

NOTE.—Spectral types in this and the following tables are from Heras et al. (2002) and references therein.

[a] Spectral segment. (SEW) Strecker et al. (1979); (HW) Hinkle et al. (1995), Wallace & Hinkle (1996, 1997); (S) SWS (Sloan et al. 2003); (CVF) ISOCAM CVF (Engelke et al. 2004); (A) *autoshape* (see text). The number in brackets is the wavelength (in microns) at which that segment ends. The first segment starts at 1 μm and is produced with *autoshape*. Where available, the Strecker et al. (1979) data cover 1.2–2.36 μm; otherwise, *autoshape* is used. The SWS spectra all start at 2.36 μm. Adjacent segments start where the previous segment ends.

[b] Photometry sources. (*MSX*) Price et al. (2004); (DIR) Smith et al. (2004); (H) Hammersley et al. (1998); (S) Selby et al. (1988); (*IRAS*) Beichman et al. (1988); (T) Tokunaga (1984).

MSX photometry with *ISO* spectra to produce an improved set of infrared calibration spectra. Section 2 gives an overview of our results; § 3 describes the data processing; § 4 presents a single-parameter function *autoshape*, which was developed to fit the measured spectra and to create spectral templates for stars with good photometry but no spectra. Section 5 compares the stellar parameters derived with *autoshape* to those in the literature; § 6 discusses the uncertainties in the derivations; and § 7 summarizes our results.

2. NEW CALIBRATED REFERENCE SPECTRA

The model spectral energy distributions used by Cohen et al. for Vega and Sirius (Sirius is scaled here by 1.01; see Price et al. 2004 for details) are adopted for this analysis in order to preserve the Cohen et al. absolute zero-magnitude flux scale in our work, even though Short Wavelength Spectrometer (SWS) measurements were available for these two primary standards. The SWS spectra for Vega and Sirius are noisy and plagued by detector nonlinearities at wavelengths longer than about 7 μm. Price et al. (2004) obtained an absolute direct calibration of Sirius, and the photometry in the present analysis is referenced to this standard. Although they also directly calibrated the infrared flux of Vega, it should only be used as a standard at $\lambda \lesssim 12$ μm, as *MSX* detected flux excesses from the known debris disk at longer wavelengths. (In Paper II Cohen et al. recommended limiting the use of α Lyr below 15 μm based on *Infrared Astronomical Satellite* [*IRAS*] measurements.)

We have combined the moderate-resolution 2.36–35 μm spectra ($\lambda/\Delta\lambda \sim 400$) obtained by the SWS (Leech et al. 2003) on *ISO* with the best photometry available on Cohen et al.'s secondary and tertiary standards, which we reference to the rescaled absolute infrared spectrum of Sirius, to create absolutely calibrated moderate-resolution spectra for 33 stars, 29 of which are in the Cohen et al. calibration network. The highest quality photometry was from *MSX*, the Diffuse Infrared Background Experiment (DIRBE) on the *Cosmic Background Explorer* (*COBE*), and Hammersley et al. (1998). *MSX* and DIRBE were space-based experiments, and therefore, atmospheric effects do not affect their measurements. If needed, measurements from *IRAS*, as well as the photometric resources listed in Appendix A of Walker & Cohen (1998), were also used.

The nine secondary standards with the most accurate absolute infrared fluxes are listed in Table 1, while 24 secondary standards with greater uncertainties are listed Table 2. The stars in Table 1 are original Cohen et al. secondary standards from which they spawned the spectral templates for the stars in the calibration network. Eighteen of the 24 stars in Table 2 had previously been assigned spectral templates in Paper X; β Peg, a Cohen et al. secondary standard with a composite spectrum, is relegated to Table 2 because it is a small-amplitude variable star in the infrared (Price et al. 2004). The derived parameters of effective temperature $T_{\rm eff}$ and angular diameter θ and their associated errors are listed in the tables and are discussed in § 5. References for the photometry and spectroscopy used to create the improved spectra are also given in the tables.

The absolute spectral energy distributions for the stars in Table 1 were constructed using precise photometry from *MSX* and DIRBE. Because the stars are bright, they also have high signal-to-noise ratio (S/N) SWS spectra over much of the wavelength range. Walker & Cohen (2002) created a template spectrum for one of these stars, β UMi, that they then used as the representative K4 III template. We have replaced this template with an SWS spectrum to 17 μm, so an absolutely calibrated measured spectrum is now available for this star. *MSX* obtained precision photometry on β Gem, and it is included in Table 1 even though it does not have an SWS spectrum. The SWS spectra of θ Cen and δ Eri, two stars of similar spectral classification to β Gem, were averaged and adopted as the composite 2.36–9 μm spectrum, to which was seamed the 9–16 μm ISOCAM circular variable filter (CVF) spectrum of δ Dra to extend the measurements to 16 μm. The result is in excellent relative agreement with the high-quality *MSX* photometry.

Table 2 contains secondary standard stars that, for a variety of reasons, have larger uncertainties in their derived absolute fluxes compared to those in Table 1. The increased uncertainty may arise, for example, from greater uncertainty in the photometry. For instance, Walker et al. (2004) estimate a 6%–9% uncertainty in the *IRAS* 12 and 25 μm photometry, which is about 10 times larger than that for the *MSX* photometry. It could also be due to lower S/N in the SWS spectra, which limits the range over which the spectra can be used, as is indicated in the tables. Two of the original Cohen et al. secondary standards have been relegated to Table 2:

TABLE 2
Additional Secondary Standards

Star (1)	Spectral Type (2)	$T_{\rm eff}$[a] (K) (3)	θ[a] (mas) (4)	Spectra[b] [to λ (μm)] (5)	Photometry[c] (6)
α^1 Cen	G2 V	5870 ± 4%	8.51 ± 2%	P[2.36], S[9], A[35]	B, E, Th
β Dra	G2 II	5100 ± 8%	3.35 ± 5%	SEW, S[9], A[35]	DIR, 2M, *IRAS*
δ Dra	G9 III	4950 ± 8%	3.35 ± 5%	S[10], CVF[16], A[35]	H, *IRAS*
δ Eri	K0 IV	4900	2.48	S[9], A[35]	B, C, VdB, *IRAS*
θ Cen	K0 III	4800 ± 4%	5.46 ± 2%	S[9], A[35]	DIR, B, C, VdB, *IRAS*
α UMa	K0 IIIa	4790	6.68	SEW, S[9], A[35]	DIR, Ken, *IRAS*
ξ Dra	K2 III	4570	3.09	S[10], A[35]	H, S, *IRAS*
α Ari	K2 III	4500 ± 4%	6.89 ± 2%	S[9], A[35]	*MSX*, DIR, A, CX
γ And	K3 IIb	4200 ± 4%	7.96 ± 2%	SEW, S[10], A[35]	DIR, A, *IRAS*
α Tuc	K3 III	4200 ± 4%	6.19 ± 2%	S[15], A[35]	DIR, C, *IRAS*
λ Gru	K3 III	4200	2.82	S[11], A[35]	C, *IRAS*
σ Oph	K2 II	4100 ± 8%	3.52 ± 5%	S[10], A[35]	DIR, H, *IRAS*
δ Psc	K5 III	4050	3.75	S[12], A[35]	DIR, S, VdB, *IRAS*
γ Phe	K4/5 III	3950	6.76	S[10], A[35]	DIR, *IRAS*
H Sco	K5 III	3850 ± 8%	4.90 ± 5%	S[11], A[35]	DIR, C, *IRAS*
δ Oph	M1 III	3850	10.23	S[13], A[35]	DIR, C, *IRAS*
AE Cet	M1 III	3850	5.19	S[11], A[35]	DIR, F, *IRAS*
δ Vir	M3 III	3660	10.71	S[11], A[35]	DIR, Ken, *IRAS*
ρ Per	M4 II	3540	15.50	S[19], A[35]	DIR, A, *IRAS*
π Aur	M3 II	3500 ± 8%	9.05 ± 5%	S[10], A[35]	DIR, K, *IRAS*
β Peg	M2.5 III	3490 ± 8%	17.88 ± 5%	SEW, S[35]	*MSX*, DIR, H, S
β Gru	M5 III	3480	27.80	S[26], A[35]	DIR, Th, *IRAS*
GZ Peg	M4 III + A2 V	3450	7.82	S[20], A[35]	DIR, Ker, *IRAS*
δ^2 Lyr	M4 II	3300 ± 8%	11.50 ± 5%	S[27], A[35]	DIR, *IRAS*

[a] Except where noted, the uncertainty in $T_{\rm eff}$ is ±6%, and that in θ is ±3%.
[b] Spectral segment. (P) Pickles (1998); (SEW) Strecker et al. (1979); (HW) Hinkle et al. (1995), Wallace & Hinkle (1996, 1997); (S) SWS (Sloan et al. 2003); (CVF) ISOCAM CVF (Engelke et al. 2004); (A) *autoshape* (see text). The number in brackets is the wavelength (in microns) at which that segment ends. The first segment starts at 1 μm and is produced with *autoshape*. Where available, the Strecker et al. (1979) data cover 1.2–2.36 μm; otherwise, *autoshape* is used. The SWS spectra all start at 2.36 μm. Adjacent segments start where the previous segment ends.
[c] Photometry sources. (A) Alonso et al. (2000); (*MSX*) Price et al. (2004); (DIR) Smith et al. (2004); (F) Feast et al. (1990); (Ken) Kenyon (1988); (Ker) Kerschbaum & Hron (1994); (H) Hammersley et al. (1998); (S) Selby et al. (1988); (*IRAS*) Beichman et al. (1988); (VdB) Van der Bliek et al. (1996); (Th) Thomas et al. (1973); (B) Bouchet et al. (1989, 1991); (C) Carter (1990, 1993); (CX) Paper X; (2M) 2MASS (Strutskie et al. 2006).

β Peg because it is a low-amplitude variable star and α^1 Cen because we replaced the model spectrum from Paper VI with a calibrated SWS spectrum that has good-quality data to 9 μm. The table also includes δ Dra. Although this star was not included in the Cohen et al. calibration network, Cohen created a calibrated template spectrum for it for use as an *ISO* calibration standard.[4] The 9–16 μm ISOCAM CVF (Blommaert et al. 2003; Engelke et al. 2004) calibrated spectrum of δ Dra is spliced onto the shorter wavelength SWS spectral segments. The CVF spectrum for this star has a much higher S/N than the SWS data but at much lower spectral resolution. The δ Dra spectrum is an important tie point for the warm-temperature end in the analysis of the trends in the stellar continua and the molecular absorption profiles. To anchor the definition of these trends at the cool end, a calibrated spectrum for β Gru, a bright southern M5 III star, is derived even though this star is a low-amplitude variable. β Dra was not in the Cohen et al. network but is included here because it has both an SWS spectrum and a high-quality near-infrared spectrum (Strecker et al. 1979), and it provides information on the sparsely populated early G spectral classes for this analysis. Finally, Walker et al. (2004) recently noted that δ^2 Lyr has little infrared variability and should provide reasonably "accurate and reliable" calibration; because it has a good-quality SWS spectrum, it too is included in Table 2.

[4] See http://www.iso.vilspa.esa.es/users/expl_lib/ISO/wwwcal/.

3. DATA PROCESSING

3.1. *Rationalizing the SWS Spectrometry*

The *ISO* SWS obtained over 1250 full-range 2.36–45 μm spectra on more than 900 objects. About 50 of these spectra are of objects most suitable as calibration references: infrared nonvariable stars without excess emission from circumstellar dust. The SWS data are available from the *ISO* data archive in the form of the 288 individual spectral segments that were obtained during a single observation (288 = 12 detectors × 12 spectral bands × 2 scan directions). The archive also has both the single spectrum created by Sloan et al. (2003) from the 288 spectral fragments for each observation and the separate segments they created for each of the 12 bands. Sloan et al. flat-fielded the measurements, removed glitches that typically arise from cosmic-ray hits, and then smoothed and resampled the spectrum onto a standard uniform wavelength grid.

The SWS was originally calibrated against several of the same Cohen stellar standards with composite spectra, such as γ Dra, that are upgraded in the present analysis. A mean relative spectral response for the spectrometer was determined from the SWS observations of a small number of Cohen et al. primary and secondary standards, as well as other stars with model atmosphere spectra. The relative response thus derived was scaled to absolute values with calibrated photometry obtained by the *ISO* program for that purpose (Hammersley et al. 1998; Hammersley &

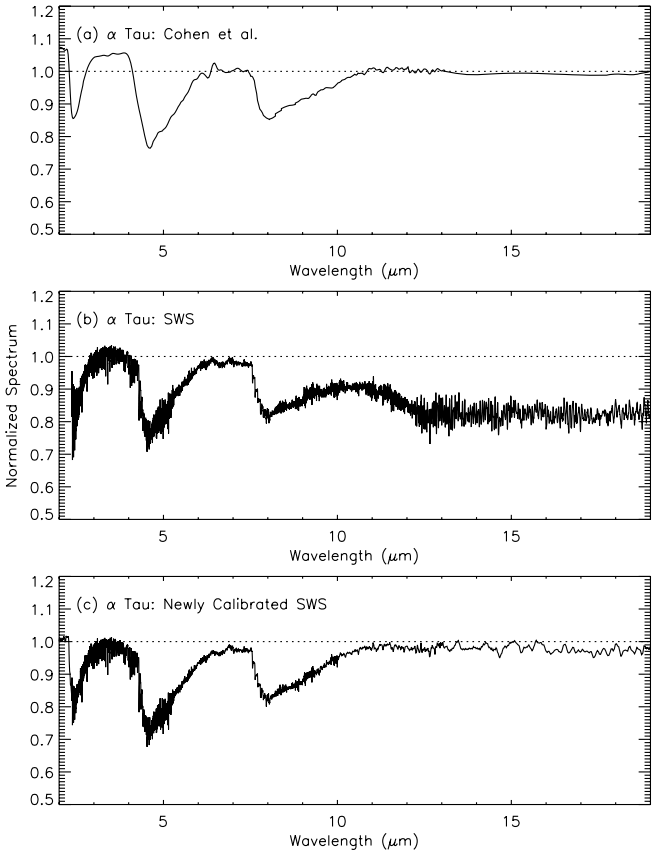

FIG. 1.—Comparison of the normalized mid-infrared spectra of α Tau. (*a*) Composite spectrum from Paper II. (*b*) SWS spectrum from Sloan et al. (2003) with the calibration from the SWS pipeline, ver. 10.1. (*c*) Recalibrated SWS spectrum from this work. All three spectra have been normalized with an Engelke function at $T_{\rm eff} = 4050$ K and $\theta = 21.01$ mas.

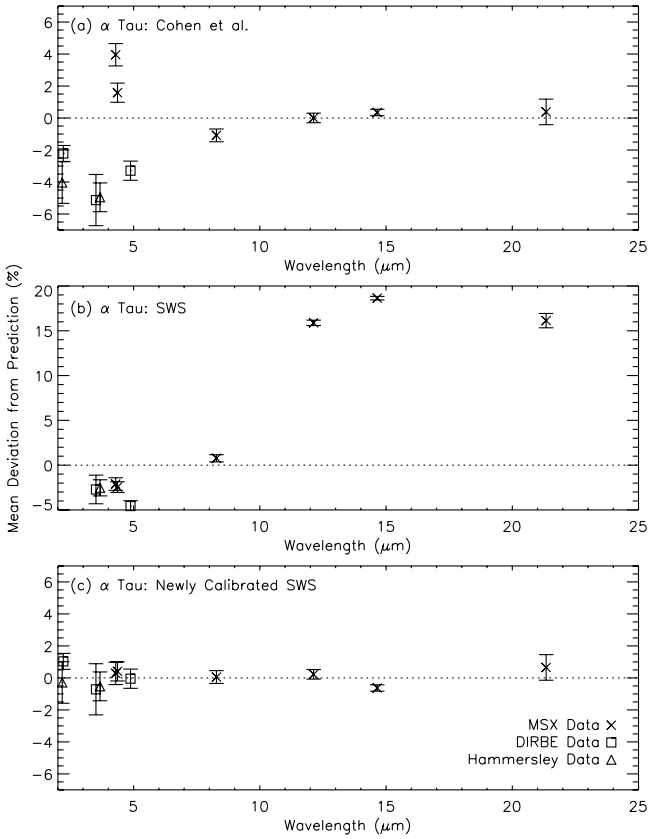

FIG. 2.—Comparison of the observed photometry for α Tau to that predicted from the spectra shown in Fig. 1, normalized to Sirius. (*a*) Percent difference for the Cohen et al. spectrum shown in Fig. 1*a*. (*b*) Percent difference for the SWS spectrum shown in Fig. 1*b*. (*c*) Percent difference for the final recalibrated SWS spectrum shown in Fig. 1*c*. The crosses show the *MSX* photometry, the squares are from DIRBE, and the triangles are from Hammersley et al. (1998).

Jourdain de Muizon 2003). The SWS team estimated that the relative spectral response has an overall uncertainty of ~10% but has larger uncertainties of ~20%–30% at the longest wavelengths (Leech et al. 2003).

Sloan et al. (2003) spliced the 12 SWS spectral segments measured on an object to form a single spectrum by assuming that the differences between segments in the regions of overlap were either additive or multiplicative. However, noise or the poor responsivity in the overlap regions, as well as incorrect assumptions about the scaling, could cause the final spectrum to depart from the correct values, occasionally by as much as 10%–20% at the band edges. Therefore, for a given star, we start with the 12 discrete spectral segments from Sloan et al. (2003). These segments are the average of all the "up" and "down" spectra from each of the 12 detectors in the sub-band, which improved the S/N by a factor of about 5 over that from a single scan. The Sloan et al. spectral segments still contain residual instrumental artifacts, due to factors such as residuals left by the nonlinear response correction or imprecise background subtraction, which are identified and removed in the present analysis. Also, the spectra become increasingly noisy beyond 8 μm, especially for the fainter stars in Table 2.

The stellar flux decreases by more than 4 orders of magnitude across the 2.36–45 μm spectral range spanned by the SWS. The first step is therefore to "flatten" the SWS spectrum by dividing out an approximate continuum. We approximate the infrared stellar continuum, as many others have done (e.g., Heras et al. 2002; Onaka et al. 2003; Marengo et al. 1999), with the Engelke function (Engelke 1992). This function is based on the semiempirical solar spectrum of Vernazza et al. (1976) and is scaled to the effective temperature $T_{\rm eff}$ and angular diameter θ for a given star:

$$F_s(\lambda, T_{\rm eff}) = 11,910\Omega\lambda^{-5} \times \left\{\exp\left[\frac{19,500}{\lambda T_{\rm eff}(1+79450/\lambda T_{\rm eff})^{0.182}}\right]-1\right\}^{-1} \text{ W cm}^{-2}\ \mu\text{m}^{-1}, \quad (1)$$

where $\Omega = \pi(\theta/2)^2$ in steradians. This function is a good representation of the stellar continuum at wavelengths $\lambda > 2$ μm for stars of solar temperature or lower. Price et al. (2004) found that the Engelke continua reproduced the *MSX* photometry on the calibration stars to a few percent.

This normalization conveniently scales the entire spectrum to a single well-resolved plot and increases the visibility of the small-scale local trends and other discrepancies that may be present. Although the errors due to background subtraction, splicing, and uncorrected nonlinearities in the detector responses may be as large as 20%, they are often smaller and would be too subtle to recognize without the normalization. Note that the corrections for these effects described herein are applied to the un-normalized data.

The large-scale deviations in the overall shape of an SWS spectrum are corrected using the assumed continuum function as a guide. Then the spectrum and/or the 12 individual SWS spectral segments are brought into agreement with the accurate infrared photometry by iteratively removing artifacts and making finer scale adjustments in the continuum. Figures 1 and 2

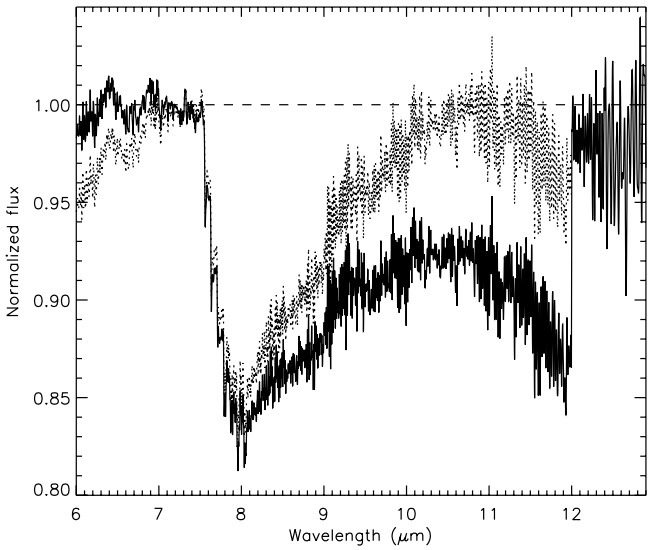

FIG. 3.—Adjustments to α Tau in the SWS spectral segment 2C, which contains the SiO fundamental. The discontinuity at 12 μm between SWS bands 2C and 3A is likely due to the nonlinear response of the detectors or an oversubtraction of the background. Two potential corrections for the discontinuity are derived by (1) adding a corrective background constant or (2) multiplying the spectral fragment by $\lambda^{0.2}$, normalized such that the correction factor is 1.0 at 7.3 μm. The two corrections are indistinguishable and overlap as the gray dotted lines in the figure. (This discontinuity does not appear in Fig. 1*b*, as that shows the band-to-band normalized spectrum, whereas for this work we start with the non-band-normalized spectral segments [Sloan et al. 2003].)

graphically demonstrate the before and after results for α Tau, the first standard for which Cohen et al. created a composite spectrum (Paper II).

Figure 1*a* shows the Cohen et al. α Tau composite spectrum after it has been divided by an Engelke function with an effective temperature of 3898 K (the effective temperature adopted in Paper II for this star), Figure 1*b* shows the similarly normalized SWS spectrum from Sloan et al. (2003), and Figure 1*c* shows our final corrected spectrum. The near-infrared portion of the Cohen et al. spectrum ($\lambda < 4$ μm) is higher than the Engelke reference, a common feature in many of the Cohen et al. spectra. Similarly, the long-wavelength portions of the normalized SWS spectra are also often lower than the Engelke reference ($\sim$20% lower in the α Tau example).

Figure 2 shows the analogous comparisons between the measured photometry and that calculated from the spectra shown in Figure 1. Significant deviations between the measured and predicted photometry occur for the Cohen et al. composite spectrum (Fig. 2*a*) at wavelengths below 5 μm. The photometric comparison using the Sloan et al. spectrum (Fig. 2*b*) shows it is in good agreement with the measured photometry in the near-infrared but is discordant by nearly 20% at wavelengths greater than $\sim$10 μm, which is consistent with the large uncertainty that Leech et al. (2003) assign to the SWS calibration at the longer wavelengths. Finally, Figure 2*c* shows that the deviations of the measurements from the predictions in our final calibrated spectrum have been reduced by using the photometry to adjust the SWS spectral segments. The processing steps used to create the final spectrum are summarized here and described in detail in the following subsections.

Some of the normalized SWS spectra, such as that of α Tau in Figure 1*b*, show systematic trends with respect to wavelength. These trends often occur near the transitions between the 12 spectral fragments. Figure 3 shows the adjustment that was necessary for one particular SWS segment of α Tau (band 2C) that lies within the SiO fundamental band. The solid line shows the segment after the Sloan et al. initial normalization. The end of the segment is about 20% below where continuity arguments with the continuum approximation say it should be. This deficit is the reason why the flux from the longer wavelength spectrum of this star in Figure 1*b* is systematically low. The droop in this spectral segment likely is due to incomplete correction of the nonlinear detector response, possibly compounded by oversubtraction of the background. The deviation can be corrected by either (1) adding a constant to the background (70 Jy in this case) or (2) multiplying by a weak function of wavelength, here $(\lambda/7.3)^{0.2}$. The values of the offset or the exponent in the λ^n expression vary with the wavelength range and the star under consideration, but the corrections that we derive from the two approaches are essentially the same. The exponent n is generally small; the largest value used for any spectral segment for any of the stars is $\sim$0.4. We chose to use the λ^n form of the correction for the general method of reshaping individual segments for its ease of application and because it can account naturally for problems produced by variations in response. The dotted lines in Figure 3 show the results of applying the corrections to the α Tau spectral segment; the two (superposed) corrections are indistinguishable.

Residual trends and offsets with respect to the normalized continuum are corrected in a piecewise fashion for a given spectral segment or group of consecutive segments. The corrected stellar spectrum was thereby initially made to conform, to within a few percent, to the Engelke function near 4, 7, and 11 μm, that is, in regions outside of the well-defined absorption bands.

Because the spectral energy distributions for stars fall steeply with wavelength, the SWS spectra become quite noisy at the longest wavelengths, even for the brightest objects. The spectra beyond $\sim$10 μm are smoothed and resampled at a gradually increasing wavelength interval in order to preserve a respectable S/N, albeit at the expense of a somewhat degraded spectral resolution. We chose to use a wavelength-dependent grid spacing for the final spectra, with a wavelength interval given by $(0.0001/1\ \mu\text{m})\lambda^2$, which provides for 10,000 samples over the 1–35 μm spectral range. The step size at 2.36 μm equals 0.02% of the wavelength ($\lambda/\Delta\lambda \sim 4400$), and the steps are 0.34% of the wavelength at 35 μm ($\lambda/\Delta\lambda \sim 300$). Depending on the observing speed, the inherent SWS resolution is $\lambda/\Delta\lambda \sim 500-2000$ at 2.4 μm and $\lambda/\Delta\lambda \sim 200-500$ at 35 μm (Leech et al. 2003).

The spectral range over which SWS data are used is indicated by the designation S[λ] in column (5) of Tables 1 and 2. The SWS coverage begins at 2.36 μm and ends at the wavelength specified within the brackets. The notation "CVF" indicates that data from the ISOCAM CVF are used for δ Dra and β Gem. Where smoothing does not sufficiently reduce the noise, a predicted spectral energy distribution derived with the *autoshape* templating procedure (described in § 4) is substituted, indicated by "A[35]" in that column. Cohen et al. analogously substituted an Engelke function for the noisy or missing long-wavelength portion of their spectral composites and templates.

3.2. *Splicing the Near-Infrared Data to the SWS Spectra*

The long-wavelength side of the *K* band and DIRBE band 2 just overlap with the 2.36 μm lower limit to the SWS spectra, while the DIRBE band 1 analog to the *J* band and the Hammersley et al. (1998) *J* and *H* photometric data lie at wavelengths much less than the SWS limit. In order to make use of the near-infrared photometry to adjust the absolute flux levels, the calibrated spectra are extended to wavelengths shorter than the SWS limit by

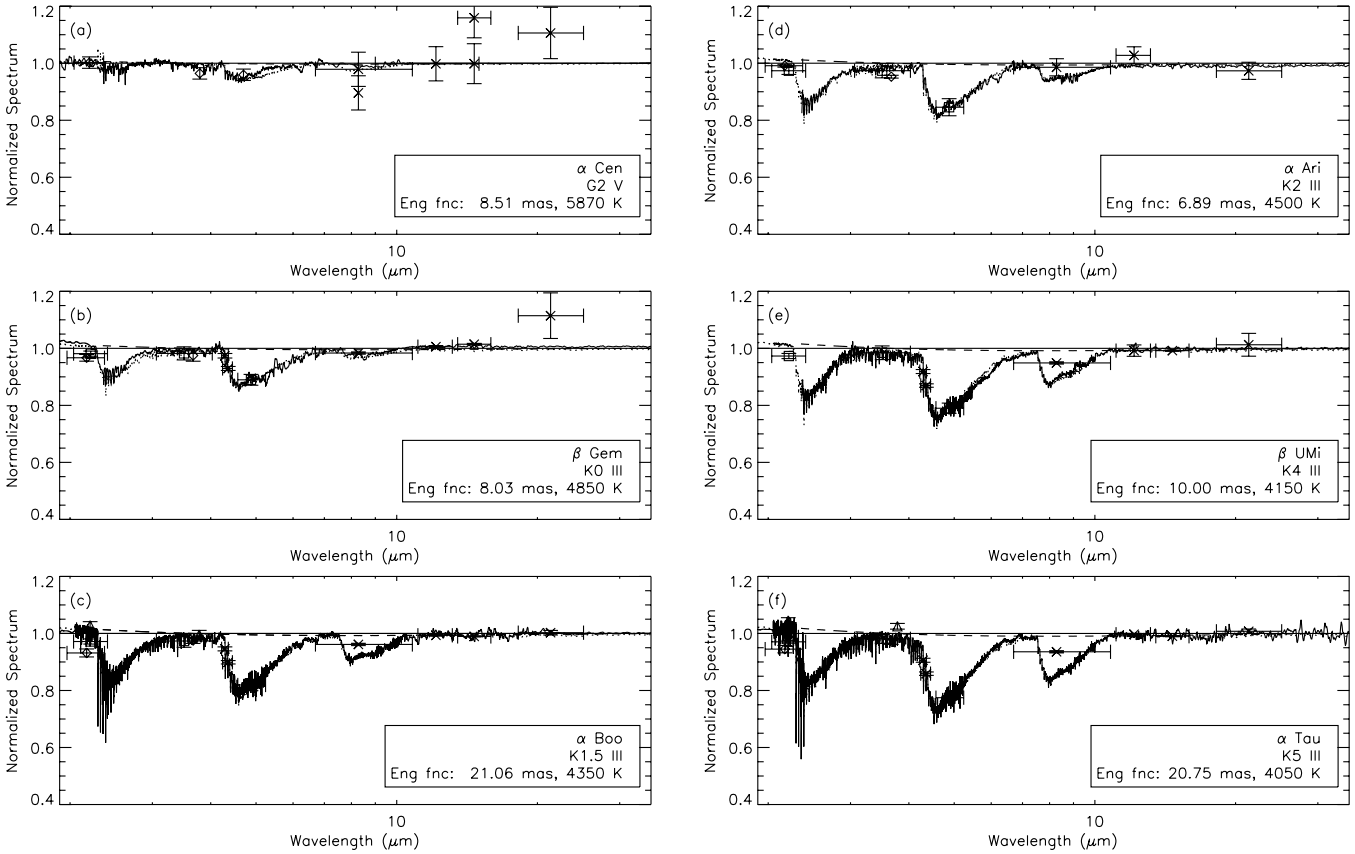

FIG. 4.—Calibrated SWS spectra (*solid lines*) for 12 stars ordered by decreasing effective temperature and normalized by eq. (1) (i.e., the Engelke function) with the appropriate temperature and angular size. The dashed lines show the continuum estimates from eq. (2). The dotted lines show the *autoshape* spectrum for the star. The photometric uncertainties (1 σ) are denoted by the vertical error bars for each measured value, and the horizontal bars indicate the >50% response of the filter.

seaming the low spectral resolution ($\lambda/\Delta\lambda \sim 70$) 1.22–2.4 μm absolute spectra that Strecker et al. (1979) obtained from the NASA Kuiper Airborne Observatory (KAO) and Lear Jet Observatory. The eight stars in Tables 1 and 2 with such spectra are indicated by "SEW" in column (5) (Strecker et al. also obtained spectra for Vega and Sirius, which are not included, as we adopt model spectra for these stars). Prior to splicing, the Strecker et al. spectra are first renormalized to the adopted flux of Sirius from Price et al. (2004). Higher resolution ($\lambda/\Delta\lambda \sim 3000$) 2.02–2.41 μm spectra from Wallace & Hinkle (1997) for α Tau, γ Dra, and μ UMa are impressed on the Strecker et al. spectra for these three stars, while the same is done for α Boo with the data from Hinkle et al. (1995). For those stars without Strecker et al. data, a pseudo-spectral energy distribution based on the Strecker et al. data and near-infrared photometry are used to extrapolate below the SWS spectrum to shorter wavelengths.

3.3. *Photometric Scaling*

The rationalized spectral energy distribution is then iteratively adjusted to bring it into agreement with high-quality photometry on the star. We have two resources for accurate photometry that were not available to Cohen et al. when they created the calibration scale and network. The first is the *MSX* photometry (Price et al. 2004), which provides a much needed longer wavelength lever arm for the absolute flux calibration of the spectra. The second is the photometry in the DIRBE Point Source Catalog (Smith et al. 2004). Cohen (1998, Paper IX) confirmed that the DIRBE photometry is entirely consistent with their established zero-magnitude flux and used DIRBE photometry to add tertiary standards to their network. In decreasing order, the preference for photometry with which we scale the spectra is *MSX*, DIRBE, Hammersley et al. (1998), Selby et al. (1988), and, for the secondary standards in Table 2, the photometry used by Cohen et al. (e.g., that in Appendix A of Walker & Cohen 1998). Although the DIRBE data set is both exo-atmospheric and extensive, its usefulness for the present analysis varies widely across the sample of stars. Since the DIRBE detectors were large, 42′ instantaneous fields of view, the stellar measurements often contain background emission that degrades the quality of data for the fainter stars. In addition, contributions from nearby stars can only be separated out for measurements in specific scan geometries. Smith et al. (2004) rejected contaminated scans from the photometry, but this frequently produced too few scans at the longer wavelengths to provide good photometry. For these reasons, we only use the DIRBE near-infrared photometry from bands 1–4 (i.e., $\lambda < 5$ μm).

The initial absolute spectral energy distribution of a star is weighted by the spectral response of the filters used for the photometric observation, and the results are integrated over wavelength to obtain a predicted absolute flux in each band. These integrated in-band fluxes are divided by the corresponding integrated in-band fluxes of the Sirius model spectrum. The resulting ratios between the star and Sirius in that band are then compared to the ratios actually measured by *MSX*, DIRBE, Hammersley et al. (1998), etc. (e.g., Fig. 2 for α Tau).

If there is a significant (>3 σ) discrepancy between the calculated and measured ratios, the stellar spectrum is modified to bring the photometric predictions into better agreement with a given measurement. These discrepancies may be small in absolute

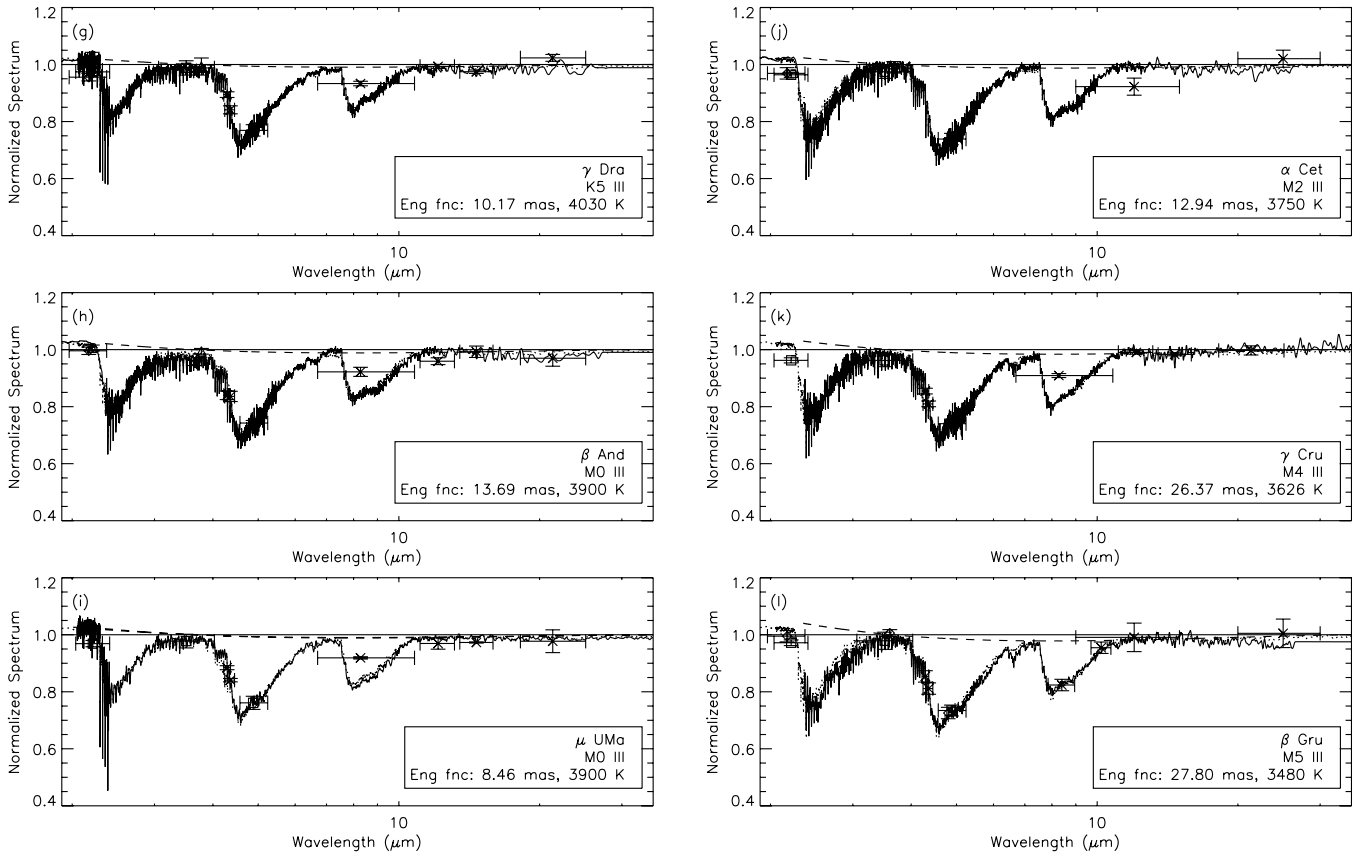

FIG. 4.—*Continued*

terms. For example, the uncertainty in the relative *MSX* photometry we use is, for the most part, less than 1% and in many cases less than 0.5%. The types of adjustments applied are as follows:

1. If the trends show a systematic wavelength dependence indicative of an incorrect effective temperature assumed for the star, then the effective temperature in the normalization (i.e., the Engelke function) is adjusted.

2. If the discrepancies show a uniform bias independent of wavelength, then the angular size is modified.

3. If the discrepancy is limited to a specific range of wavelengths, then the spectral segment(s) in that region is (are) raised or lowered as the photometry indicates. The scale factor that is used to rationalize the overlap between the segments being pieced together has a rather large uncertainty because of the poor responsivity at the edges of the SWS segments, and adjacent segments are often rich in stellar lines, particularly at the shorter wavelengths. Since the segments also often have slightly different resolutions, the "best" scaling factor to combine the overlap regions is somewhat ambiguous. The λ^n correction applied to a segment can also be changed slightly to include relatively small local corrections if these are within the measurement uncertainty.

4. If the star is bright enough to have both a well-measured spectrum and high-quality photometry, the departure of the spectrum from the analytic approximation to the continuum is adjusted such that the low-frequency changes in the slope of the spectral continuum with wavelength [Δ(continuum)/$\Delta\lambda$] are the smallest necessary to provide a good fit to the photometry. A modified continuum, discussed in § 4, is used for the fainter stars that have less complete photometry.

Since the measured and predicted photometry for each of the stars are expressed relative to Sirius, the absolute calibration of the final spectrum is directly tied to the absolute spectral energy distribution of Sirius. If the detailed Sirius model that we adopt from Paper I (modulo 1.01) were revised, then each final spectrum in this analysis could easily be revised as well.

Figure 4 shows the absolute spectra for the 12 stars with the most accurate photometry and/or the most extensive SWS wavelength coverage. The spectral types range from G2 to M5 and are displayed in order of decreasing effective temperature or later spectral type, where $T_{\rm eff}$ is that determined from our fitting and the spectral type is from Heras et al. (2002) and references therein. Overlain on each plot is the photometry with error bars used to adjust the spectra. The horizontal bars indicate the bandwidth of the filters for each photometric measurement.

4. THE CONTINUUM AND SPECTRAL TEMPLATES

The continua of the calibrated spectra of the stars in Figure 4 were interactively adjusted to follow the absolute photometry. There are subtle systematic differences, increasing with decreasing temperature, between the final calibrated stellar spectra shown in the figure and the corresponding Engelke function. For example, the spectra in later type stars do not rise back to the reference level defined by the Engelke function ($y = 1$; Fig. 4, *solid horizontal line*) between the molecular absorption bands, such as at 7 μm. On the other hand, the continuum increasingly rises above the reference level at shorter wavelengths as the effective temperature is decreased.

From the 12 stars in Figure 4, we have derived an empirical correction to the Engelke function for $\lambda > 2.36$ μm that is a better approximation to the continua. The shape of the continuum in the modified function is defined by a single input parameter, the effective temperature $T_{\rm eff}$. The significant infrared features in the SWS spectra that arise from the molecular absorption by CO and

TABLE 3
TEMPLATED STANDARD STARS

Star (1)	Spectral Type (2)	$T_{\rm eff}$[a] (K) (3)	θ[a] (mas) (4)	Spectra[b] [to λ (μm)] (5)	Photometry[c] (6)
α Aur	G4: III:	5450	10.23	A[35]	DIR, *IRAS*
α Hya	K3 II–III	4150	9.59	A[35]	DIR, B, C, *IRAS*
γ Aql	K3 II	4050	7.29	A[35]	DIR, H, S, T
α TrA	K2 II	4000	9.81	A[35]	DIR, C, *IRAS*
ϵ Car	K3 III + B2 V	3300 $\pm$ 10%	14.59 $\pm$ 10%	A[35]	DIR, C, *IRAS*, 2M

[a] The uncertainty in $T_{\rm eff}$ is $\pm$7%, and that in θ is $\pm$4%. Note that the uncertainties in $T_{\rm eff}$ and θ are not independent. The overall absolute flux uncertainty is usually close to the uncertainty cited for θ.
[b] Spectral segment. (A) *autoshape* (see text).
[c] Photometry sources. (DIR) Smith et al. (2004); (H) Hammersley et al. (1998); (S) Selby et al. (1988); (*IRAS*) Beichman et al. (1988); (B) Bouchet et al. (1989, 1991); (C) Carter (1990, 1993); (T) Tokunaga (1984); (2M) 2MASS (Strutskie et al. 2006).

SiO are also found to be well parameterized as functions of the effective temperature. We have created a deterministic procedure called *autoshape*, described in the following sections, based on the correlation of such key features with effective temperature from the averages of the individually calibrated spectra.

Autoshape can be used to create spectral templates for a continuum of effective temperatures and has been effectively validated for spectral types between G2 and M5. Since this approximation uses averaged data from 12 stars, the *autoshape* results are influenced less by random measurement error or by aberrant features that might be introduced by adopting a single template to represent an entire spectral type. We substitute the appropriate *autoshape* data for noisy or missing spectral portions for stars that have SWS data (Tables 1 and 2), use the function to make templates for stars with good photometry but no SWS spectra (Table 3), and derive estimates of temperature and angular diameter when good stellar photometry is available (§ 5).

4.1. *The Shape of the Continuum above* 2.36 μm

The deviations between the calibrated spectra of the stars in Figure 4 and the respective Engelke function continua arise from a variety of factors, such as sources of opacity other than H^- free-free absorption. The Engelke function incorporates an ad hoc analytic approximation for the wavelength dependence of the measured disk integrated brightness temperature of the Sun (Engelke 1992). This was extrapolated to lower effective temperatures assuming the infrared opacity is solely due to H^- free-free absorption. In the derivation of the function, it was also assumed that the $T(\tau)$ relationship for the star is approximated by $T(\tau) = T_{\odot}(\tau)(T_{\rm eff}/T_{\odot})$. Carbon & Gingerich (1969) validated this assumption over the temperature range 4000–6000 K.

Atmospheric modeling could, perhaps, provide better estimates for the stellar continua than the Engelke function. The detailed models include a more exact treatment of opacity and the variation of temperature with optical depth, as well as the gravitational effects that Decin et al. (2004) suggest are necessary to reproduce the detailed *Spitzer Space Telescope* Infrared Spectrograph (IRS) calibration spectra. Thus, we examined the infrared spectra generated with detailed stellar atmosphere models and found that the deviations from the Engelke continuum are similar to those observed in the normalized, recalibrated SWS spectra in Figure 4. Figure 5 shows the normalized difference between the flux from a Kurucz α Boo model atmosphere at 4300 K[5] and the corresponding Engelke function (the sharp drop at $\lambda < 1.6$ μm is due to the inapplicability of the Engelke function below this wavelength, as it marks the transition from H^- free-free being the dominant opacity source to bound-free absorption dominating).

The model should include more of the applicable physics in the stellar atmosphere than the Engelke function. However, the Engelke function is actually in better agreement with the available spectroscopy and photometry on α Boo, particularly in the near-infrared, than either the Kurucz model atmosphere shown in Figure 5 or the earlier models for this star used by Cohen et al. (e.g., Paper VII). The 11 other fiducial stars qualitatively show the same deviations, both positive and negative, as seen in Figure 5 but at a smaller amplitude. The dashed lines shown in Figure 4 are the best scaling of the deviation in Figure 5 that fits the photometry. These corrections tend to increase with decreasing temperature of the star. Thus, the photometry for $\lambda > 2$ μm can be brought into agreement by simply adding a scaled version of the deviations in Figure 5 to equation (1).

Figure 6 shows that an inverse linear function of the effective temperature provides a good fit to the scaling factors needed to adjust the "excess" for the 12 fiducial stars in Figure 4. The dashed line in the figure is the linear least-squares fit to the data

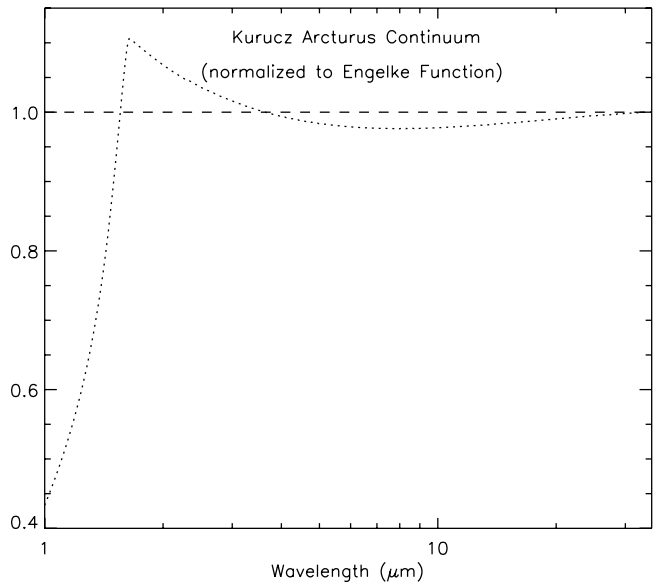

FIG. 5.—Percent deviation of the Kurucz model continuum for α Boo ($T_{\rm eff}$ = 4300 K) from the Engelke function for the same temperature.

[5] See http://kurucz.harvard.edu/stars/ARCTURUS/.

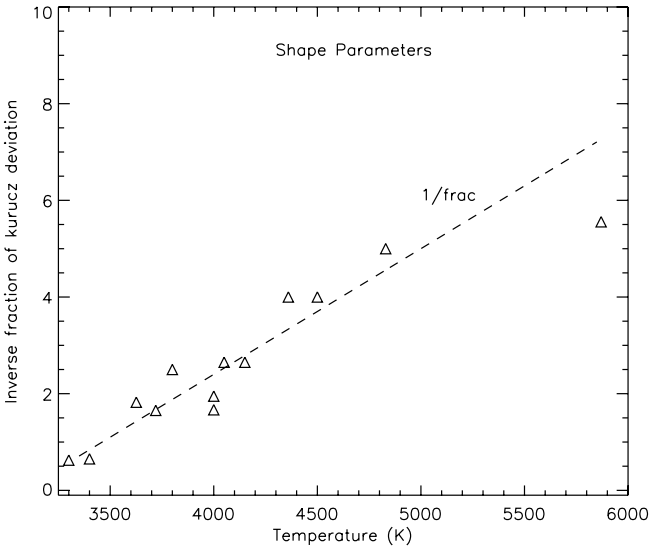

FIG. 6.—Inverse of the correction factor (1/frac) to eq. (1) vs. the effective temperature of the star. The fractional correction is the amount of deviation of the α Boo continuum in Fig. 5 needed for the continuum estimates in Fig. 4 (*dashed lines in that figure*). The linear fit through the data is shown by the dashed line $0.0026 \pm 0.0003T_{\rm eff} - 7.99 \pm 1.08$, which is used in eq. (2). (If the G star at $\sim$5900 K, which is somewhat of an outlier and has a relatively small correction, were neglected in the fit, the line fit would be $0.0027T_{\rm eff} - 8.38$.)

of $0.0026T_{\rm eff} - 7.99$. For wavelengths greater than 2.36 μm, the continuum used in *autoshape* is the Engelke function plus the excess in Figure 5 divided by the scale factor

$$f(\lambda \geq 2.36\ \mu\text{m}) = \text{Eng}(\lambda, T_{\rm eff}) \times \left\{1 + \frac{[\text{Kur}(\lambda, T_{\alpha\ \text{Boo}})/\text{Eng}(\lambda, T_{\alpha\ \text{Boo}})] - 1}{0.0026T_{\rm eff} - 7.99}\right\}, \quad (2)$$

where $\text{Eng}(\lambda,T_{\rm eff})$ is given in equation (1) and $\text{Kur}(\lambda,T_{\alpha\ \text{Boo}})$ is the Kurucz model for α Boo at $T_{\alpha\ \text{Boo}} = 4300$ K. Note that the numerator in the correction factor is the same for all spectra.

The maximum corrections are small, $\sim$3% or less for wavelengths greater than 2.5 μm. Equation (2) scales the deviations at $\lambda > 2.36$ μm in Figure 5 by about 0.2 for a K0 star, 0.5 for K4, and 1.0 for M4.

4.2. *Molecular Absorption versus Effective Temperature above* 2.36 μm

The molecular absorption features in the spectra also show trends with effective temperature and, equivalently, spectral type. Absorption profiles for the CO and SiO fundamental and overtone bands have been extracted from the calibrated SWS spectra for the 12 stars in Figure 4 after normalizing their spectra with the continua defined by equation (2). The 12 individual profiles for each of the four molecular bands are averaged to obtain the mean absorption profiles shown in Figure 7. These mean absorption

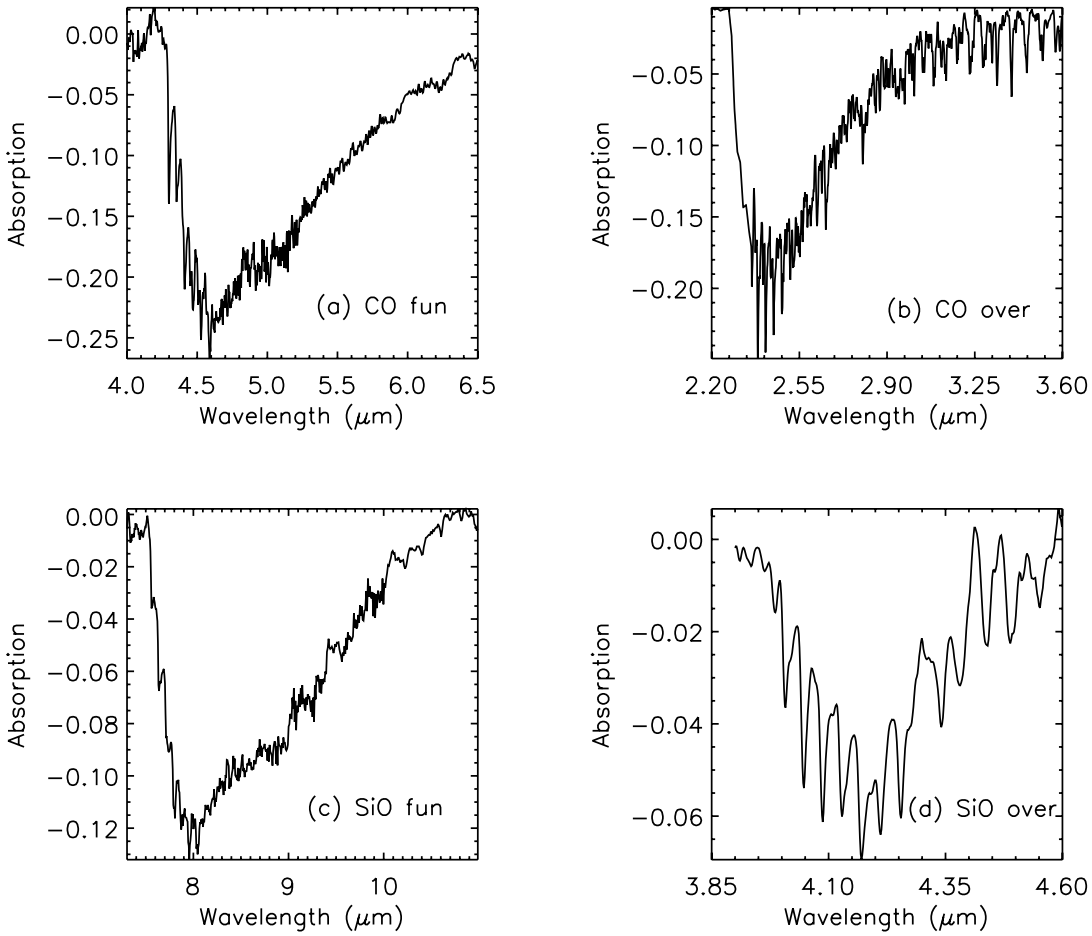

FIG. 7.—Averaged molecular absorption profiles. (*a*) CO fundamental profile averaged over the spectra in Fig. 4. A correction has been applied to remove the contribution of the SiO overtone at 4.2 μm (see text). (*b*) Average profile for the CO first overtone. (*c*) Average SiO fundamental profile. (*d*) Average SiO overtone profile.

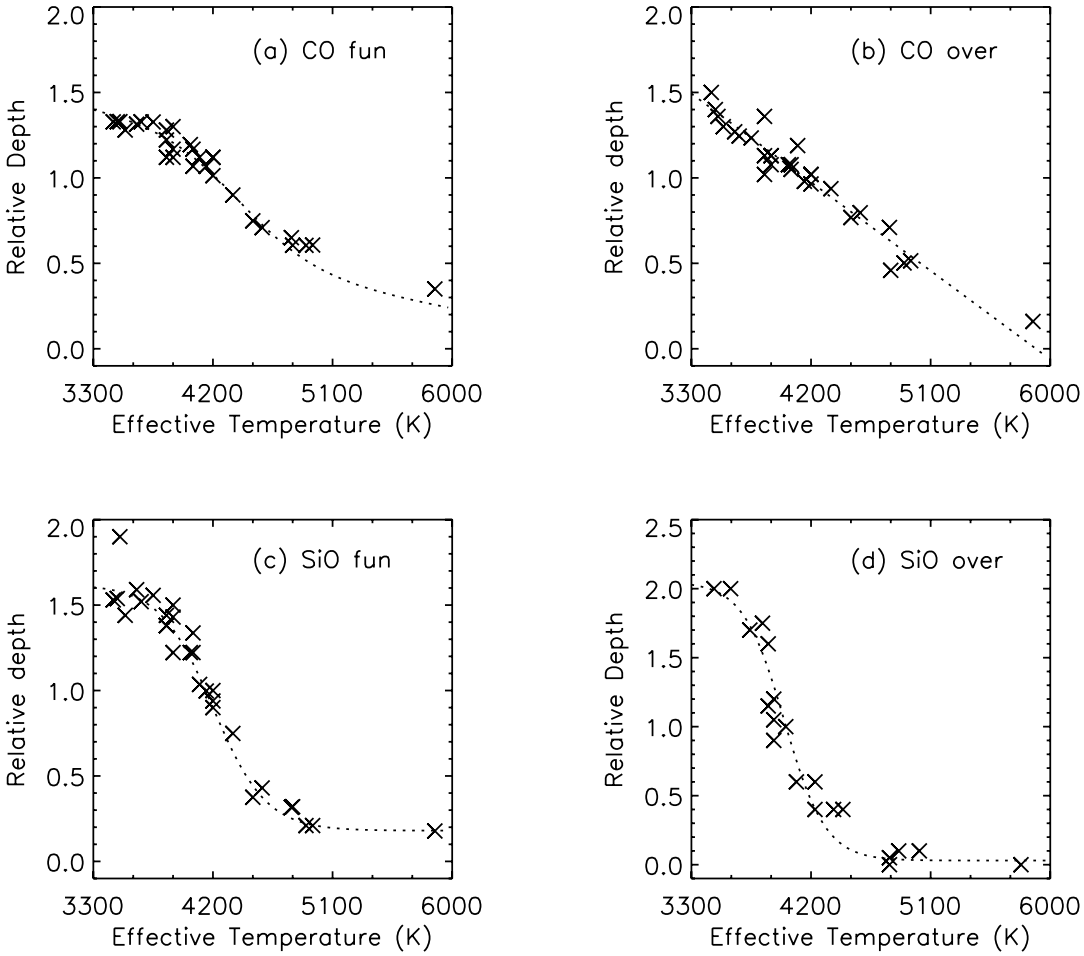

FIG. 8.—Scaling factors needed to fit the profiles in Fig. 7 to the stars from Tables 1 and 2 as a function of $T_{\rm eff}$ for (*a*) the CO fundamental profile, (*b*) the CO first overtone, (*c*) the SiO fundamental, and (*d*) the SiO first overtone.

profiles are then scaled to fit the actual profiles of each star with an absolutely calibrated SWS spectrum in Tables 1 and 2. The scale factors obtained are plotted against the derived effective temperatures of these stars in Figure 8.

The CO absorption bands and the SiO fundamental are extracted from the normalized spectra in a straightforward fashion. The SiO overtone, however, has to be extracted from the edge of the CO fundamental by taking differences between the averaged spectra of the relatively warm stars (Figs. 4*a*–4*e*) and the cooler stars (Figs. 4*f*–4*l*). The higher temperature stars seem to exhibit little SiO overtone absorption and can be scaled relative to the spectra of the cool stars such that the CO fundamental is removed by the subtraction, thus leaving the SiO overtone.

The scale factors for the CO overtone in Figure 8 show an approximately linear decrease with increasing effective temperature, while those for the other molecular bands exhibit more complex behavior. For these bands, little variation in the rather small absorption is observed above a particular temperature unique to each band. The absorption linearly increases with decreasing temperature below that unique temperature, and then the features all saturate at a temperature of about 3800 K, which produces an S-shaped curve. The dotted lines in Figure 8 are analytic functions of $T_{\rm eff}$ that are fitted to the data: a linear function for the CO first overtone and a hyperbolic tangent function plus a linear tail for the other three bands. Cohen & Davies (1995, Paper V) examined the equivalent width of the SiO fundamental and found similar results (cf. their Fig. 10). This S-shaped dependency is also apparent in the equivalent width analysis of the molecular bands by Heras et al. (2002), as can be seen in their Figures 5 and 6. Aringer et al. (1997) provide a theoretical foundation for this behavior in the SiO overtone as a function of effective temperature and gravitational acceleration. Thus, our results are in good qualitative agreement with the work of others.

The average absorption profiles in Figure 7 can be multiplied by the scale factors in Figure 8 to fit the measured profile for a star at a particular $T_{\rm eff}$. A quantitative comparison with other work can be made by rescaling the *y*-axes in Figure 8 to indicate either the maximum absorption depth at the band head for each star or the equivalent width of the molecular absorption. For example, the maximum absorption depth of the molecular features in the individual stars would be represented by the curves in Figure 8 if the ordinates were multiplied by the feature minima in Figure 7, that is, by $\sim$0.25 for the CO fundamental, 0.22 for the CO overtone, 0.13 for the SiO fundamental, and 0.065 for the SiO overtone.

To obtain equivalent widths, the plots in Figure 8 must be multiplied by the integrated area within each absorption band. For quantitative comparison with Heras et al. (2002), the integration has to be limited to the narrow limits within each band that they adopted. By comparing corresponding points on our Figure 7 and their Figures 5 and 6, we initially estimated the integrated areas to be 0.08, 0.011, 0.13, and 0.009 μm for the CO fundamental, the CO overtone, the SiO fundamental, and the SiO overtone, respectively.

Integrating the CO fundamental between the 4.30 and 4.70 μm limits used by Heras et al. produces an integrated area of 0.08 μm, which is the value we had estimated visually. The scale factor to convert the *y*-axis of Figure 8*a* to equivalent widths for the entire 4.0–6.7 μm range spanned by the CO fundamental band (after removing the SiO overtone) is 0.289 μm. The conversion factor to integrated area over the 2.38–2.45 μm range used by Heras et al. for the CO overtone is 0.013 μm, and the equivalent width of the entire CO overtone band shown in Figure 8*b* is 0.096 μm. However, this width includes the 3.02–3.40 μm region, which Heras et al. note is affected by OH absorption. They do not derive equivalent widths for OH but note that it appears in stars as early as K0 and is prominent in the M stars. Integrating over the Heras et al. 7.60–9.00 μm limits to the SiO fundamental, we derive a factor of 0.137 μm to convert Figure 8*c* to equivalent width; the equivalent width of the entire band is 0.203 μm. Integrating the SiO overtone over the 4.10–4.30 μm range adopted by Heras et al. gives 0.0095 μm and an equivalent width of 0.018 μm. Thus, the present profiles and the analysis by Heras et al. are in excellent quantitative agreement.

The agreement is not surprising, as we analyzed about two-thirds of the same stars used in the Heras et al. study. However, our spectral rationalization does result in smaller scatter about the trends. Since Heras et al. (2002) found the same correlations as we but for a 50% larger sample of stars, the more precise trends that we derive also apply to the larger data set and, by inference from the random nature of the criteria used to select these stars for SWS observation described by Kraemer et al. (2002), to the general population of giant stars with spectral types G2 and later.

4.3. *Spectra below* 2.36 μm

Because of the discontinuity at 1.6 μm in the spectra of stars cooler than ~6000 K (apparent in Fig. 5), a different normalization function is needed to account for the trends in the 1.22–2.5 μm spectral range of the Strecker et al. (1979) data. We use equation (1) between 1.6 and 2.36 μm and append a blackbody with a variable brightness temperature for the 1.0–1.6 μm spectral region. The brightness temperature increases from $T_b = T_{\rm eff}$ at 1.0 μm up to the higher brightness temperature of the Engelke function at 1.6 μm; T_b follows a wavelength dependence of the form $(\lambda - 1.0)^2$ between these two boundary values. This functional form is based on the Strecker et al. stellar continua (after adjusting them to the quality photometry), as well as theoretical models (e.g., those of Kurucz).

The eight Strecker et al. (1979) spectra from the KAO for stars in Tables 1 and 2 are separated into two groups: three "warm" stars (β Dra, α UMa, and β Gem) and five "cool" stars (α Boo, γ And, α Tau, β And, and α Cet). The data are normalized by the extrapolation described above with the angular sizes and temperatures determined from *autoshape* fits to the data at $\lambda > 2.36$ μm. Based on the depths of the CO and SiO bands, the equivalent temperature of the average normalized warm stellar spectrum is 4900 K (the simple average of the derived individual temperatures of the stars is also about 4900 K). Similarly, the averaged cool star spectrum has a temperature equivalent of 4040 K. We model the (normalized) near-infrared segment of *autoshape* with a linear interpolation in $T_{\rm eff}$ of the difference between the two average spectra divided by their temperature difference:

$$f_{\rm NIR,normalized} = {\rm hot}(\lambda) + (4900 - T_{\rm eff})\,\frac{{\rm cool}(\lambda) - {\rm hot}(\lambda)}{4900 - 4040} \quad (3)$$

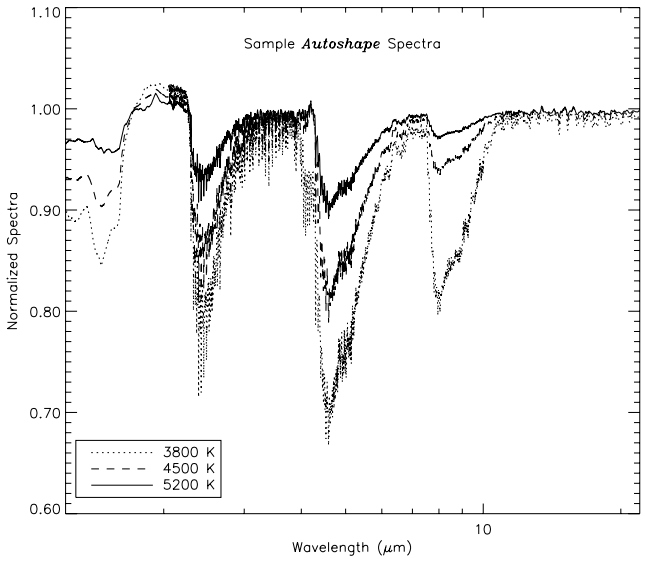

FIG. 9.—*Autoshape* function for three different temperatures. The functions are normalized to the appropriate Engelke function at $\lambda > 1.6$ μm and by a blackbody with a brightness temperature that varies as a quadratic function of wavelength, from the stellar effective temperature at 1.0 μm to the temperature of the appropriate Engelke function at 1.6 μm. The strengthening of the CO and SiO fundamental and overtone bands as the temperature is decreased is readily apparent, as is the $\Delta v = 1$ CN red-band system between 1.4 and 1.6 μm and the CO second overtone at 1.6 μm; Price (1970) discussed the temperature dependence of these features. The normalization overestimates the continuum flux for the stars for $\lambda \gtrsim 1.8$ μm, accounting for the depression in the normalized spectra at the shorter wavelengths.

for 1.22 μm $< \lambda <$ 2.36 μm. To test equation (3), the resulting spectra were compared to our renormalized Strecker et al. data with satisfactory results.

4.4. *Autoshape: Application for Spectral Templates*

The corrections and scaling that created the calibrated spectra for the 12 fiducial stars shown in Figure 4 are strongly constrained over the entire mid-infrared wavelength range by the accurate *MSX*, DIRBE, and Hammersley et al. (1998) photometry. Except at the longest wavelengths, this procedure creates spectra for these 12 stars from observed data without appeal to model constructs. The Engelke function is used only for trend and continuity processing of the SWS data. It is more difficult, however, to constrain global shapes for the fainter stars to which Cohen et al. applied spectral templates. Many of these stars, including those in Table 2, have only a few photometric measurements. Also, the uncertainty in continuum shape will be larger for stars that have significant reddening. Fortunately, Walker & Cohen (2002) found that a reddening correction was necessary for only two of the stars in Table 2: 0.03 mag for δ Oph and 0.42 mag for π Aur.

We use the trends found in the 12 fiducial stars to develop the empirical procedure *autoshape* so as to constrain the revisions to the SWS data for the stars in Table 2 that have only moderate-quality mid-infrared photometry from *IRAS* (for which Walker et al. [2004] estimate a 6%–9% photometric accuracy). *Autoshape* combines the continuum defined by equation (2) with the average absorption profiles for the CO and SiO fundamental and overtone bands (Fig. 7) scaled to the effective temperature of a given star using the correlation shown in Figure 8. Equation (3) allows us to extend the spectrum from 2.36 down to 1.22 μm. The single input parameter to the *autoshape* algorithm is the effective temperature, $T_{\rm eff}$. Figure 9 shows examples of normalized spectra produced with *autoshape* at three effective temperatures.

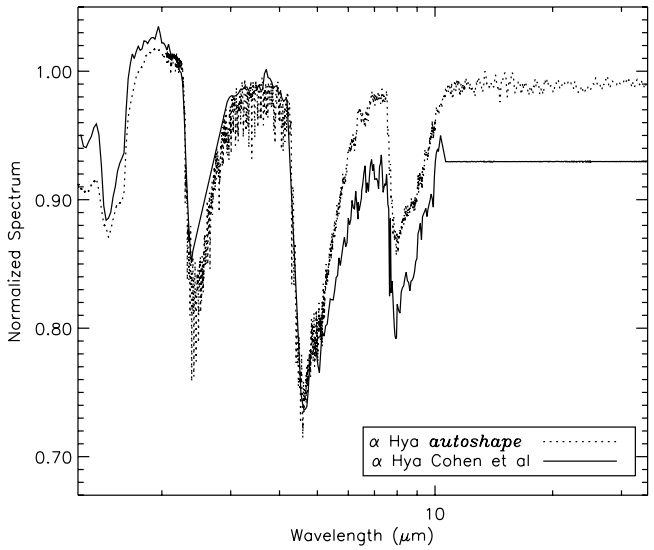

FIG. 10.—*Autoshape* spectrum for α Hya (*dotted line*) compared with the spectral template from Paper X (*solid line*).

The spectrum derived from *autoshape* for the effective temperature of a given star is projected as a scaffold on which the SWS segments, if available, can be overlain. For those stars with little spread in their photometry, the depths of the SWS absorptions are the basis for estimating the effective temperature. Then, the angular size of the star is obtained by multiplying equation (2) at the derived temperature by the normalized spectrum and scaling the result to match the observed fluxes. The *autoshape* prediction is also substituted for noisy or otherwise unusable SWS spectra beyond 10 μm for many of the fainter secondary standards in Table 2. This is similar to the Cohen et al. substitution of Engelke functions for noisy or missing spectra beyond 13 μm.

We used the *autoshape* routine to create spectral templates for α Aur and γ Aql to test the efficacy of the procedure. As a historical note, Low (1973) performed one of the first direct mid-infrared stellar calibrations against α Aur, as well as α Tau and β And. *Autoshape* templates were also created for three Cohen et al. secondary standards that do not have SWS measurements, α Hya, α TrA, and ϵ Cen, in order to provide improved spectral resolution for all the original Cohen et al. secondary standards. Figure 10 compares the results for α Hya to the Cohen et al. spectral template for this star. The *autoshape* routine can be used to create higher resolution and more accurate templates for all of the stars in the infrared stellar calibration network (Paper X). Table 3 lists stars for which we created spectral templates.

As exemplified in Figure 1, Cohen et al.'s spectra and the templates derived therefrom have systematically higher flux in the $\sim$1–5 μm spectral region than the absolute spectra in this paper and the derivative *autoshape* templates. This discrepancy has also shown up in the recent literature. Cohen et al. (2003, Paper XIII) created template spectra for faint standards to calibrate the Infrared Array Camera (IRAC) on *Spitzer*. In their calibration of IRAC, Reach et al. (2005) noted a systematic 5%–7% difference between the camera calibration against the A stars compared to that from the K stars; they decided to use only the A stars for calibration. The discrepancy disappears when we repeat the step-by-step analysis described by Reach et al. (2005) using the appropriate *autoshape* templates. Thus, caution should be exercised when using Cohen et al.'s faint template spectra for calibration, particularly with cool stars (e.g., Ishihara et al. 2006).

5. DERIVED PARAMETERS

The stellar effective temperature and angular diameter can be derived by fitting *autoshape* to the absolutely calibrated spectrum of the star. These quantities are listed in columns (3) and (4), respectively, in Tables 1–3. The uncertainties are estimated by interactively varying the parameters until the fits, such as that shown in Figure 2*c*, obviously start to fail. For many of the stars in Table 2, the overall spectral shape is poorly constrained by the photometry. Therefore, the relationship between the band depth and effective temperature for the CO fundamental (Fig. 8*c*) is used to estimate the temperature. This typically gives limits of $\pm$3% for the temperature range 3800 K $< T_{\rm eff} <$ 5000 K with somewhat larger uncertainties above and below these temperatures. The corresponding limits on angular size, which depend on the uncertainties in both the effective temperature and the absolute flux, are then derived.

5.1. *Angular Diameter*

We compare the derived angular diameters to published values obtained by interferometric means in Table 4 and by indirect means in Table 5. The tables list the number of stars N in common, the average of the ratios of the derived to the published angular diameters, and the bias in the ratio. The bias is defined as $(\text{ratio} - 1)/\sigma_{\rm reduced}$, where $\sigma_{\rm reduced} = \sigma_{\rm rms}/\sqrt{N}$ and $\sigma_{\rm rms}$ is the rms deviation about the ratio average. Stars of spectral types G and K are listed separately from those with spectral type M, as a dichotomy has shown up between the two groups in some of the references.

Overall, our sizes average about 1% larger than the mean of the values found in the literature. The comparisons with published results on G- and K-type stars, however, show much less

TABLE 4
ANGULAR SIZE COMPARISON: INTERFEROMETRIC VALUES

	G–K STARS			M STARS		
REFERENCE	No. of Stars	Ratio $\pm$ $\sigma_{\rm rms}$	Bias[a]	No. of Stars	Ratio $\pm$ $\sigma_{\rm rms}$	Bias[a]
Mozurkewich et al. (2003)	10[b]	0.999 $\pm$ 0.018	0.2	9	0.979 $\pm$ 0.023	2.7
Di Benedetto & Rabbia (1987)	5	1.023 $\pm$ 0.023	2.2	2	0.976 $\pm$ 0.031	2.2
Perrin et al. (1998)	2	1.011 $\pm$ 0.006	2.6	1	0.981	...
Dyck et al. (1998; UD)	6	1.080 $\pm$ 0.070	2.8	5	1.100 $\pm$ 0.022	20
Di Benedetto & Rabbia (1987; UD)	4	1.013 $\pm$ 0.031	1.0	2	0.995 $\pm$ 0.006	1
Average (excluding UD results)		1.012 $\pm$ 0.011		10	0.979 $\pm$ 0.003	

NOTE.—UD indicates uniform disk.
[a] Bias = $(\text{ratio} - 1)/(\sigma_{\rm rms}/\sqrt{N})$.
[b] Limited to stars with less than 10% DIRBE variability; see § 6.2.

TABLE 5
Angular Size Comparison: Indirect Values

Reference	G–K Stars			M Stars		
	No. of Stars	Ratio $\pm$ σ_{rms}	Bias[a]	No. of Stars	Ratio $\pm$ σ_{rms}	Bias[a]
Decin et al. (2000)	7	1.006 $\pm$ 0.008	2.0	3	1.033 $\pm$ 0.026	2.2
Blackwell et al. (1991)	5	1.020 $\pm$ 0.009	5.0	3	1.030 $\pm$ 0.006	9
Alonso et al. (2000)	6	1.010 $\pm$ 0.015	1.6	1	1.039 $\pm$ 0.026	2.6
Manduca et al. (1981)	5	1.025 $\pm$ 0.005	11	2	1.033 $\pm$ 0.027	1.7
Di Benedetto (1998)	4	0.999 $\pm$ 0.012	0.2	0	...	...
Perrin et al. (1998)	0	...	...	3	1.049 $\pm$ 0.025	3.4
Average		1.012 $\pm$ 0.011			1.037 $\pm$ 0.008	

[a] Bias = (ratio $-$ 1)/($\sigma_{rms}/\sqrt{N}$).

scatter than the comparisons with M stars. Possible explanations for the increased discrepancy in the M star size include inappropriateness of our fitting function to M stars; limitations in the methods used in the direct measurements, perhaps relating to limb-darkening corrections (discussed below); and a lack of constancy among M stars as a group. A large disagreement for M stars is also apparent among the published angular diameters. There is, however, some pattern to the divergence between our results and those obtained in particular studies or with specific methods, such as that all M stars from a specific reference are either larger or smaller than ours. Also, there are correlations in the angular diameters obtained by similar methods in the sense that M star interferometric diameters are larger than ours, while indirect determinations produce smaller M star diameters.

5.1.1. *Interferometric Sizes*

The values that we derive for G and K stars are in good agreement with the interferometric diameters from Mozurkewich et al. (2003), Perrin et al. (1998), and Di Benedetto & Rabbia (1987) but average about 2% smaller for the M stars, particularly for stars of spectral type M2 and later. The Dyck et al. (1998) diameters are $\sim$10% smaller than our results, but their values are given for a uniform disk; the other references in Table 4 apply corrections for limb darkening using model expectations. Di Benedetto & Rabbia (1987) published both uniform disk and limb-darkened diameters. When their uniform disk values are compared to our derived values, the discrepancy between the G and K stars and the M stars is greatly reduced. This suggests that the M star differences in the interferometer measurements may be an artifact of the particular limb-darkening models being applied.

There is empirical support for the application of limb-darkening models to K and G stars but little specific as to their use with M stars. For example, Di Benedetto & Bonneau (1990) found that the visibility function for β And (M0 III) at 1.65 and 2.2 μm was inconsistent with a conventional limb-darkened disk. They proposed that the discrepancies could be explained if the star had a small bright spot. Haniff et al. (1995) observed Mira variables and found that Gaussian profiles provided a better approximation to the radial brightness profiles than did uniform disks, although, besides being much later types than our sample, these stars also show complicated and asymmetric structure.

Comparing results for individual stars: Quirrenbach et al. (1996) used the Mark III optical interferometer to measure the angular diameter of α Boo (K1.5 III) at five visual wavelengths. They found that the measured uniform disk diameters quantitatively agreed with wavelength-dependent predictions derived from the limb-darkening coefficients of Manduca (1979). Our derived diameter of 21.1 $\pm$ 0.2 mas is in good agreement with their "true limb-darkened diameter" of 21.0 $\pm$ 0.2 mas. Hutter et al. (1989) also used the Mark III to measure 24 stellar diameters, albeit before the calibration and observing techniques were well understood (Mozurkewich et al. 2003). Our agreement is good (within 1 σ) for β And (M0 III) and γ Dra (K5 III), although their α Ari (K2 III) is significantly larger than other results, including ours, which is consistent with the Mozurkewich et al. (2003) comment that the early Mark III results may overestimate the diameters.

Hajian et al. (1998) first confirmed stellar limb darkening for the K giants α Ari and α Cas (K0 III) with the Naval Prototype Optical Interferometer; subsequently, the group did so for several additional stars (e.g., Nordgren et al. 1999; Wittkowski et al. 2001). The data confirm the presence of limb-darkened radial profiles but do not yet allow model-independent determination of empirical limb-darkening profiles. The authors note that the model-dependent limb-darkening corrections are several times larger than the formal uncertainties in the interferometric observations. Our diameter of 6.89 $\pm$ 0.14 mas for α Ari is slightly higher than the limb-darkened diameter of 6.80 $\pm$ 0.07 mas they obtained but well within the uncertainties.

Kervella et al. (2003a) used the Interferometer Commissioning Instrument on the Very Large Telescope at *K* band to derive a limb-darkened diameter for α Cen (G0 V) of 8.51 $\pm$ 0.02 mas, the same value we derive. Kervella et al. (2003b) give 6.01 $\pm$ 0.02 mas for Sirius, also at *K* band. This is 1.5 σ smaller than the 6.04 mas adopted for Sirius by Cohen et al. in Paper I and 3 σ less than the size of 6.07 mas inferred by the revised flux for this star (Price et al. 2004) that we adopt in the present analysis.

Ridgway et al. (1982) made multiple lunar occultation observations on α Tau (K5 III) over a variety of wavelengths to constrain limb darkening and found a corrected angular size of 20.88 $\pm$ 0.10 mas, in good agreement with our diameter of 20.75 $\pm$ 0.21 mas. More recently, Richichi & Roccatagliate (2005) analyzed a combined set of lunar occultation and long-baseline interferometric measurements of α Tau and found an average limb-darkened diameter of 20.58 $\pm$ 0.03 mas, again within 1 σ of our value.

The discordance among limb-darkening correction factors is highlighted in studies that observed stars over a range of spectral types. Di Benedetto & Rabbia (1987) observed 11 K and M giants at *K* band with the two-telescope interferometer I2T in France. They used Manduca (1979) limb-darkening models to derive correction factors ranging from 0.975 for β Gem (K0 III) to 1.036 for β And (M0 III). On the other hand, Perrin et al. (1998) used a correction factor of 1.035 for all K1.5 through M8 stars that they studied at *K* band. This value was also based on the same Manduca (1979) models, supplemented by those of Scholz & Takeda (1987)

TABLE 6
Temperature Comparison

Reference	G–K Stars			M Stars		
	No. of Stars	Ratio $\pm$ σ_{rms}	Bias[a]	No. of Stars	Ratio $\pm$ σ_{rms}	Bias[a]
Heras et al. (2002)	18	1.01 $\pm$ 0.03	1.5	12	1.00 $\pm$ 0.03	0.4
De Jager & Nieuwenhuijzen (1987)	16	1.00 $\pm$ 0.03	0.0	12	1.05 $\pm$ 0.02	8.5
Ridgway et al. (1980)	13	1.00 $\pm$ 0.01	0.0	11	1.00 $\pm$ 0.01	0.0
Van Belle et al. (1999)	12	1.01 $\pm$ 0.03	1.2	11	1.01 $\pm$ 0.02	1.7
Mozurkewich et al. (2003)	10	1.02 $\pm$ 0.03	2.1	9	1.03 $\pm$ 0.03	3.2
Alonso et al. (2000)	6	1.01 $\pm$ 0.02	1.4	3	1.00 $\pm$ 0.03	0.2
Dyck et al. (1998)	6	0.96 $\pm$ 0.03	3.2	5	0.96 $\pm$ 0.02	5.5
Manduca et al. (1981)	5	1.00 $\pm$ 0.01	0.3	2	0.99 $\pm$ 0.03	0.4
Blackwell et al. (1991)	5	1.01 $\pm$ 0.01	1.7	3	1.01 $\pm$ 0.01	1.5
Di Benedetto & Rabbia (1987)	5	1.00 $\pm$ 0.02	0.0	2	1.04 $\pm$ 0.02	2.6
Di Benedetto (1998)	4	1.03 $\pm$ 0.02	3.3	0	...	...
Perrin et al. (1998)	2	1.02 $\pm$ 0.01	1.6	1	1.02	...
Average		1.01 $\pm$ 0.02			1.01 $\pm$ 0.02	

[a] Bias = (ratio $-$ 1)/($\sigma_{rms}/\sqrt{N}$).

for the coolest stars. Mozurkewich et al. (2003) conducted perhaps the most thorough analysis of limb darkening to date, using 85 stars with spectral types from A7 V to M6 III. They examined the variation in measured angular diameters at four visual wavelengths and compared their results with those from other groups at *K* band. They used correction factors from more recent models by Claret et al. (1995) and Diaz-Cordoves et al. (1995) to derive limb-darkened diameters from their uniform diameter measurements. At 800 nm the corrections range from about 6% at K0 to almost 10% for M4 stars; the 451 nm corrections are about 4% larger. The *K*-band corrections grow from about a 1% correction for K stars to just over 3% for the late M stars. Thus, applying a single correction value to all stars, even at *K* band, could lead to discrepancies of about 4%.

Besides the limb-darkening issue, other effects could contribute to the disagreement between our derived angular sizes and those from other analyses. In their equivalent width analysis, for instance, Heras et al. (2002) specify wavelength limits for water vapor absorption but derive no values for the corresponding equivalent width over this range. They note that model atmospheres calculated by Decin et al. (2000, 2003a, 2003b, 2003c) indicate that the water vapor absorption is broad and depresses the continua of M2–M4 stars by 2%, and by 5% for M5 stars. The fact that we do not account for water vapor absorption in developing the *autoshape* routine may contribute to the K–M discrepancies in angular diameters compared to the interferometric determinations. A simplistic view of the situation is that the continuum flux from the lower atmosphere predicted by the Engelke function is more or less uniformly depressed across the infrared by absorption due to water vapor and opacity sources other than H^-. This absorption could be (partially) taken into account by the algorithmic modifications in equation (2), which depress the mid-infrared continuum of M stars by 2%–3%. The solid angle of the star in equation (2) would then increase to compensate for any additional absorption. Thus, a 2%–5% uncompensated absorption would produce a 1%–2% low bias in the derived angular diameters.

5.1.2. *Indirect Determinations*

The angular diameters based on the indirect infrared flux model (e.g., Blackwell et al. 1991) methods are all systematically smaller than ours (Table 5). The values for the M stars are typically $\sim$4% smaller, and those for K stars are $\sim$1% smaller. A primary cause of this discrepancy is the different zero-point flux adopted for the flux calibrator used in a particular study. For example, Manduca et al. (1981) fitted models to the Strecker et al. (1979) 1.22–5 μm spectra for five of the stars in our analysis. They rescaled the Strecker et al. calibration, which was referenced to the Vega model of Schild et al. (1971), to match the Dreiling & Bell (1980) model for Vega. The resulting diameters average 3% lower than ours. This bias is primarily due to the different zero-point flux adopted for Vega by Manduca et al. (1981), which falls 3%–4% below the Vega flux adopted by Cohen et al. (Paper I) in this wavelength region. Adjusting the flux reference to the absolute flux scale of Price et al. (2004) reduces the average difference between their diameters and ours to $\sim$1.5%. Comparing our diameters to those derived by Cohen et al., the ratio for 28 stars from Tables 1–3 is 1.012 $\pm$ 0.026; they estimated 1% internal uncertainty, indicating good agreement despite the 1% flux rescaling.

The accuracy of the results derived by the indirect methods, including the current work, is directly proportional to the accuracy of the adopted absolute flux calibration. The differences in the M star results obtained from some indirect methods may reflect the calibration uncertainty of their photometry for these stars. Alternatively, we may overestimate the mid-infrared flux for the M stars (although neglect of the water vapor absorption mentioned above causes our diameters to change in the wrong direction).

5.2. *Effective Temperature*

We can also compare the effective temperatures derived from *autoshape* with those in the literature (Table 6). The agreement between the effective temperatures that we derive and those determined by others is generally quite good. For a few studies, the M stars show a larger disagreement than the earlier spectral types. Specifically, the comparisons with Mozurkewich et al. (2003) and de Jager & Nieuwenhuijzen (1987) have effective temperatures that are 3%–5% smaller than ours for the M stars, although the G–K stars match well.

Ramírez & Meléndez (2005) recently used the infrared flux method to derive temperatures and angular diameters of giant and dwarf stars. They too found that the direct methods (specifically that of Mozurkewich et al. 2003) produce lower temperatures for the M stars compared to the infrared flux method results, and they suggest that the limb-darkening correction for the interferometry may be the source of this discrepancy.

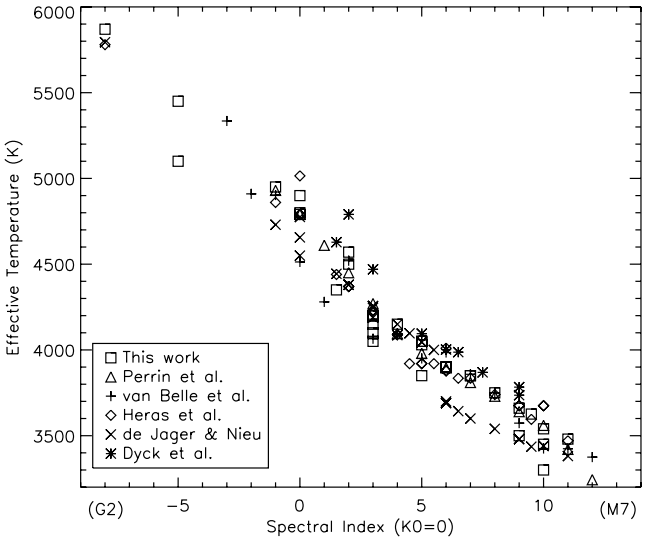

FIG. 11.—Effective temperatures vs. spectral index derived in the present work compared to those found in the literature. The spectral index ranges from −8 for spectral type G2 to −1 for G9, 0 for K0 to 5 for K5, and 6 for M0 to 12 for M6.

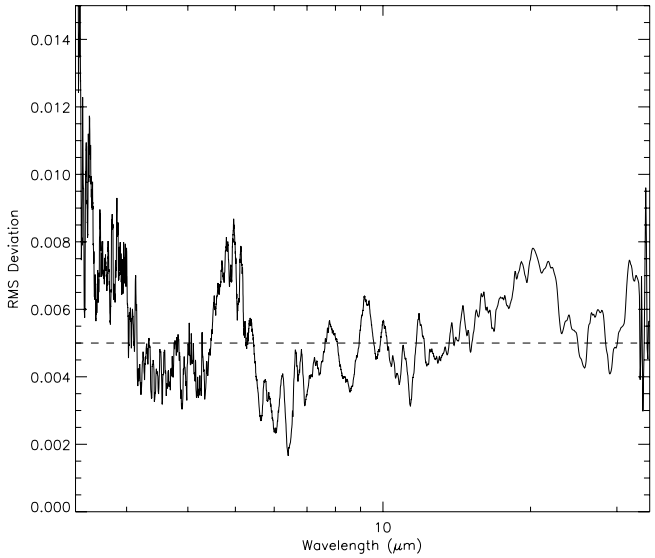

FIG. 12.—Averaged rms scatter of the deviations of the final calibrated normalized spectra of α Boo, α Tau, γ Dra, β And, and γ Cru between 2 and 35 μm from the predicted *autoshape* curves. The deviations are less than 1% over most of the wavelength range.

De Jager & Nieuwenhuijzen (1987) created an interpolation table using effective temperature and spectral types for 268 stars compiled from the literature. They included tables of temperature versus spectral type for luminosity classes I, III, and V and derived smoothly varying numerical parameters fitted to the discrete classifications. Table 6 compares the temperatures they predicted for the spectral classes present in Tables 1 and 2 with the temperatures derived here. The average ratio for K giants is 1.00 ± 0.03. As can be seen in Figure 11, the temperatures for the M giants in Tables 1 and 2 are systematically higher with respect to the de Jager & Nieuwenhuijzen values. The average ratio to M giants alone is 1.05 ± 0.02, which corresponds to a difference of about 200 K. The discontinuity in the de Jager & Nieuwenhuijzen data in Figure 11 is due to their inclusion of spectral types K7 and K9, which are not often used (e.g., Ridgway et al. 1980; Dyck et al. 1996), and probably contributes to the temperature discrepancy with our results.

Figure 11 shows our derived temperatures (Tables 1 and 2) plotted against the spectral type together with mean effective temperatures from the literature. The scatter in the comparisons is somewhat better for the spectral range G–K than for the M stars, but the agreement is consistent for the different spectral types, especially if the discordant de Jager & Nieuwenhuijzen (1987) values are excluded. We conclude that equation (2) is a good representation of the absolute emergent infrared spectral distribution of late-type stars and that its defining parameter, $T_{\rm eff}$, is the characteristic temperature of the star.

6. UNCERTAINTIES AND CAVEATS

6.1. *Estimated Uncertainties*

Price et al. (2004) derived a formal rms uncertainty of 1.1% in the direct calibration of the absolute flux for α CMa, the primary standard star we use in this analysis. In addition to this uncertainty are our uncertainty estimates in seaming the spectral fragments together and in the photometry used to scale the results to absolute fluxes.

In general, we estimate the uncertainty in the local shape to be about 5% near 1.22 μm for the *autoshape* extrapolations, 2.5% at 2.36 μm, 1% between 3 and 12 μm, and ∼2% at longer wavelengths. These uncertainties are estimated from comparisons of multiple SWS spectra on the same star, from comparisons of the spectra from different stars of same spectral type, and from the variations in the photometry used in this analysis that were obtained from different sources. Stars with several SWS observations typically require different trend corrections. The resulting profiles agree well overall, but there is a 1%–2% local disagreement on the long-wavelength side of the SiO bands. Discrepancies between the normalized spectra for two stars of a given spectral type usually are a percent or less and are rarely as large as 2%. Variation in the spectral features within a spectral class has also recently been observed in *Spitzer* IRS calibration data (Sloan et al. 2004). For stars with Strecker et al. (1979) data, we estimate the uncertainty to be ∼2% in the 1.22–2.36 μm range.

We (partially) account for water absorption by the manner in which we tie the *autoshape* function to the photometry. However, absorption by the υ_2 bending mode at $\lambda = 6.55$–6.70 μm is apparent on the wings of the CO fundamental for the cooler stars in Figure 4. There is some ambiguity as to how much water vapor absorption is present that may lead to the bias in the derived angular diameters for the cool stars. A reasonable flux bias error is ∼2%–4%, which is about half that needed to rationalize the angular diameters.

Figure 12 shows the rms of the deviations between the final absolute spectra of α Boo (K1.5 III), α Tau (K5 III), γ Dra (K5 III), β And (M0 III), and γ Cru (M4 III) and the *autoshape* results. The differences between the *autoshape* spectra and the observed, absolutely calibrated spectra are less than 1% for most of the wavelength range.

6.2. *Variability*

Several of the stars in this study are known optical variables: γ Dra, β Peg, α Cet, β Gru, and GZ Peg, for example. Except for γ Dra, which has a spectral type of K5 III, these stars have spectral types of M2 III or later. As such, they would not have fulfilled one of the Cohen et al. original selection criteria: that the secondary standard must be of spectral type M0 III or earlier to avoid the high probability that the source is variable (Paper X). Cohen et al. relaxed this criterion to M4 III in order to include γ Cru because some systems required a calibration source that

TABLE 7
DIRBE Variability

Star	Spectral Type	DIRBE Band 1 (%)	2 (%)	3 (%)	4 (%)
β Gem	K0 III	1 ± 3	1 ± 1	3 ± 3	1 ± 2
α Boo	K1.5 III	4 ± 3	1 ± 1	4 ± 2	1 ± 1
β UMi	K4 III	4 ± 3	1 ± 1	3 ± 3	2 ± 2
α Tau	K5 III	...	0 ± 1	2 ± 2	0 ± 1
γ Dra	K5 III	5 ± 3	2 ± 1	3 ± 2	2 ± 2
μ UMa	M0 III	3 ± 3	1 ± 1	3 ± 3	3 ± 3
β And	M0 III	2 ± 3	...	...	1 ± 1
α Cet	M2 III	3 ± 3	1 ± 1	3 ± 3	3 ± 2
γ Cru	M4 III	4 ± 3	0 ± 1	3 ± 2	2 ± 1
α^1 Cen	G2 V	5 ± 3	...	1 ± 6	...
β Dra	G2 II	5 ± 4	4 ± 3	9 ± 7	10 ± 10
δ Dra	G9 III	2 ± 4	10 ± 3	41 ± 7	17 ± 6
δ Eri	K0 IV	2 ± 5	3 ± 6	11 ± 9	16 ± 16
θ Cen	K0 III	...	1 ± 2	7 ± 5	6 ± 5
α UMa	K0 IIIa	5 ± 3	1 ± 1	5 ± 2	3 ± 3
ξ Dra	K2 III	4 ± 5	10 ± 2	11 ± 4	24 ± 8
α Ari	K2 III	3 ± 3	1 ± 1	5 ± 3	4 ± 3
γ And	K3 IIb	2 ± 3	2 ± 1	3 ± 3	3 ± 3
α Tuc	K3 III	3 ± 3	2 ± 2	3 ± 4	4 ± 4
λ Gru	K3 III	6 ± 5	4 ± 5	7 ± 8	13 ± 17
σ Oph	K3 II	4 ± 4	5 ± 4	10 ± 7	10 ± 12
δ Psc	K5 III	8 ± 4	6 ± 3	7 ± 5	14 ± 10
γ Phe	K4/5 III	3 ± 3	...	...	6 ± 4
H Sco	K5 III	...	...	19 ± 11	10 ± 13
δ Oph	M1 III	...	1 ± 1	4 ± 3	1 ± 2
AE Cet	M1 III	3 ± 3	...	...	3 ± 5
δ Vir	M3 III	3 ± 3	1 ± 1	2 ± 2	2 ± 2
ρ Per	M4 II	...	1 ± 1	5 ± 2	4 ± 2
π Aur	M3 II	...	...	12 ± 6	5 ± 3
β Peg	M2.5 III	5 ± 3	3 ± 1	4 ± 2	4 ± 1
β Gru	M5 III	6 ± 3	2 ± 1	4 ± 2	2 ± 1
GZ Peg	M4 III + A2 V	...	2 ± 2	6 ± 5	...
δ^2 Lyr	M4 III	2 ± 2	2 ± 1	4 ± 3	3 ± 2
α Aur	G4: III:	1 ± 3	0 ± 1	2 ± 2	2 ± 1
α Hya	K3 II–III	2 ± 3	1 ± 1	2 ± 3	2 ± 2
α TrA	K2 II	...	0 ± 2	6 ± 3	5 ± 2
ϵ Car	K3 III	3 ± 3	1 ± 1	3 ± 3	4 ± 2
γ Aql	K3 II	4 ± 4	0 ± 2	3 ± 4	5 ± 4

Note.—DIRBE bands are (1)1.25 μm, (2) 2.2 μm, (3) 3.5 μm, and (4) 4.9 μm.

was brighter than any of those in the original network. The variation in the infrared brightness of a star that is an optical variable or suspected variable is usually much less than that in the visual. Thus, only sources with small-amplitude (suspected) variability in the visual are included in Tables 1 and 2. The estimated infrared variation should be included in the total uncertainty assigned to the calibrated flux.

MSX measured a systematic 8% variation in the infrared irradiance of β Peg during the 10 month mission in 1996–1997. The amplitude and phase of the variation were well correlated across the wavelength range of 4.3–21 μm. Smith et al. (2004) also statistically detected variability in this star during the 10 month DIRBE mission (which did not overlap with the 10 month *MSX* mission). The β Peg moderate-resolution spectrum created under the present work is anchored to the median values of the *MSX* fluxes. To be conservative, a $\pm$4% uncertainty should be root-sum-squared with the $\sim$1% uncertainty in generating the spectrum and the 1.1% uncertainty in the absolute flux calibration and the result used for this star.

None of the other stars in Table 1 with *MSX* photometry were measured by *MSX* to be variable. As part of their processing to create the DIRBE point-source catalog, Smith et al. (2004) statistically assessed the variability of the bright infrared stars over the 10 month *COBE* mission. Table 7 lists the percent variability in the DIRBE photometry for bands 1–4 from this catalog for the stars in Tables 1–3, along with the uncertainty in the estimate.

Smith et al. tried to eliminate scans contaminated by extraneous sources in the beam from the analysis used to derived the variability parameters. However, as noted previously for the DIRBE mid-infrared photometry, the statistics for variability are less secure for the fainter stars. Given these difficulties we consider a source to be variable if the DIRBE variability parameter has a significance of 2 σ or greater in more than one DIRBE band. Two stars in the list, δ Dra and ξ Dra, have a large variability, greater than 10%. Neither star has *MSX* photometry. However, as mentioned earlier, δ Dra was used to calibrate the *ISO* CVF. If the DIRBE results are correct, then the CVF calibration uncertainties may be underestimated. Besides β Peg, four other stars fulfill the 2 σ variability in more than one band: α TrA, π Aur, ρ Per, and β Gru. The DIRBE variability of β Gru is somewhat smaller than for β Peg and is well detected due to the high-S/N measurements that DIRBE obtained for this star.

6.3. *Outliers*

The derived temperatures for ϵ Car and δ^2 Lyr are anomalously low for their spectral types; ϵ Car (K3 III) is a double star, but any contamination from the hotter B2 V should bias the derived temperature high. Interstellar reddening would bias the temperature low, as would very thin circumstellar emission, although Cohen et al. use zero reddening in Paper X for ϵ Car. Regardless of the cause of this anomaly, the final calibrated spectrum of ϵ Car fits the infrared photometry to $<$5%. The source δ^2 Lyr (M4 II) is also cooler than the other M4 stars in our sample (Table 2). It is relatively faint, however, and has correspondingly higher uncertainty in the temperature estimate; thus, it is only 1 σ below the expected value of $T_{\rm eff} \sim 3500-3600$ K.

7. SUMMARY

We have improved the spectral resolution and absolute accuracy for 10 of the Cohen et al. secondary standards and replaced the α^1 Cen model and the templated spectrum of β UMa with absolutely calibrated observed spectra. The moderate-resolution *ISO* SWS spectral fragments for these stars from Sloan et al. (2003) were scaled to accurate infrared radiometry from *MSX* and DIRBE. Low-resolution near-infrared spectra from Strecker et al. (1979) for nine stars were seamed onto the SWS spectra after correcting the data set to the Price et al. (2004) absolute flux for Sirius, the primary standard used in this study. We adopted the absolute fluxes and model spectra proposed by Cohen et al. in Paper I for Vega and Sirius (scaled by 1.01 for Sirius) to preserve the zero-magnitude fluxes of Cohen et al. as validated by Price et al. (2004) and because the SWS spectra for these stars become noisy at $\lambda \gtrsim 7$ μm.

We have created a routine to match the continuum for the 12 standard stars as defined by the infrared photometry. This routine, *autoshape*, is a combination of the Engelke function of the appropriate effective temperature and the excess of a Kurucz α Boo atmospheric model spectrum. The amount of excess with respect to the Engelke function is well fitted by an inverse linear function in effective temperature. The absorption profiles for the CO and SiO fundamental and overtone bands are found to vary smoothly as a function of effective temperature. An analytic function was

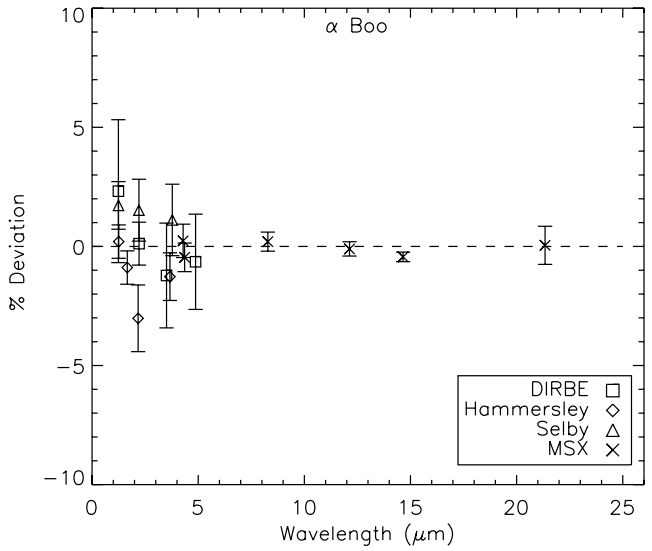

FIG. 13.2. Final photometric fit for α Boo.

FIG. SET 13.—Final photometric fits for the stars in the sample. [*See the electronic edition of the Astronomical Journal for* Figs. 13.1–13.38.]

derived that, when combined with the *autoshape* continuum, produces a representative infrared spectrum for any given spectral type. A pseudocontinuum was created for wavelengths shorter than the 2.36 μm lower limit of the SWS based on the Strecker et al. (1979) spectra to extend the *autoshape* predictions to 1.2 μm for the stars without Strecker et al. data. The *autoshape* routine was used to generate spectral templates for three of the original Cohen et al. secondary standards that do not have SWS spectra (α Hya, α TrA, and ϵ Car). A template for the fourth such secondary standard, β Gem, was created by combining the SWS and CVF spectra of θ Cen, δ Eri, and δ Dra, which are of the same spectral class as β Gem, with the *autoshape* template and scaling the results to the high-quality *MSX*, DIRBE, and Hammersley et al. (1998) photometry.

Absolute infrared spectra for an additional 21 fainter secondary standards were created by combining their SWS spectra with *autoshape* predictions over the spectral region in which the SWS data were too noisy to yield useful information and with the best available photometry. Of these fainter secondary standards with SWS data, only α Ari also had *MSX* photometry. All of the stars have high-quality DIRBE measurements in at least two DIRBE bands, although seven stars were noted by Smith et al. (2004) to vary by more than 10% in at least one of the bands. The spectra generated here for all 33 stars will be made available via CDS.

The estimated 1 σ absolute uncertainties in the secondary standards vary with wavelength. They are generally 1%–2% but can be as high as about 5% at $\sim$1 μm for spectra that rely on *autoshape*. The minimum uncertainty is dominated by the absolute accuracy in the *MSX* photometry (Price et al. 2004). Variability in some of the stars in Tables 1 and 2 has been noted, and the amplitudes of the variability have to be folded into the flux uncertainty estimates. The uncertainties in the spectra of the fainter secondary standards are higher and reflect the paucity of high-quality infrared photometry available for these stars.

The effective temperatures and angular diameters of the stars were derived by the infrared flux method using *autoshape* for the stellar source function. The good agreement between the effective temperatures that we derive and those in the literature attests to the fact that *autoshape* provides good approximations to the relative infrared spectral energy distributions, even for cool M giants. However, the opacity sources that become significant for the cool stars, such as water vapor absorption, may bias the derived angular diameters to being too low.

We wish to thank the referee R. Gehrz for helpful comments that improved the manuscript. This research has made use of NASA's Astrophysics Data System Bibliographic Services, data products from the Two Micron All Sky Survey (2MASS), which is a joint project of the University of Massachusetts and the Infrared Processing and Analysis Center/Caltech funded by NASA and the NSF, and the SIMBAD database, operated at CDS, Strasbourg, France.

APPENDIX

PHOTOMETRIC SCALING OF THE CALIBRATED SPECTRA

This appendix contains information on the adjustments that were used to rationalize the spectra and to scale the result to absolute values for each of the stars in Tables 1–3. The stars are listed in the order that they appear in the tables. The adjustments, photometric scaling, and derived parameters are listed for each star. Plots for each star (Fig. Set 13) display the measured photometry against what is predicted from the absolute spectrum. As an example, the parameters, photometry (Table 8), and plot for α Boo (Fig. 13.2) are included here; the rest are available in the electronic version of the *Astronomical Journal*.

The *ISO* SWS spectra we used were the averaged spectral fragments given by Sloan et al. (2003), and the listed adjustments are applied to those fragments as described in the main text. The short-wavelength spectra from Strecker et al. (1979) are seamed onto the SWS with the listed adjustments. Additional short spectral fragments from other resources were used for a small number of stars as noted.

For convenience, the photometric magnitude scale for a given photometric reference was adjusted so that $[IR_{Sirius}] = -1.36$. The DIRBE photometry was taken from Smith et al. (2004), but

TABLE 8
α BOO PHOTOMETRY

Band	Magnitude	Reference
DIRBE 1	-2.221 ± 0.030 (0.04 ± 0.03)	Smith et al. (2004)
DIRBE 2	-2.988 ± 0.009 (0.01 ± 0.01)	Smith et al. (2004)
DIRBE 3	-3.083 ± 0.022 (0.04 ± 0.02)	Smith et al. (2004)
DIRBE 4	-2.934 ± 0.020 (0.01 ± 0.01)	Smith et al. (2004)
J	-2.198 ± 0.007	Hammersley et al. (1998)
H	-2.853 ± 0.007	Hammersley et al. (1998)
K	-2.964 ± 0.014	Hammersley et al. (1998)
L	-3.097 ± 0.010	Hammersley et al. (1998)
J	-2.22 ± 0.02	Selby et al. (1988)
K	-3.05 ± 0.02	Selby et al. (1988)
L	-3.14 ± 0.02	Selby et al. (1988)
MSX A	-3.140 ± 0.004	Price et al. (2004)
MSX B_1	-3.082 ± 0.007	Price et al. (2004)
MSX B_2	-3.031 ± 0.006	Price et al. (2004)
MSX C	-3.187 ± 0.003	Price et al. (2004)
MSX D	-3.182 ± 0.002	Price et al. (2004)
MSX E	-3.199 ± 0.008	Price et al. (2004)

NOTES.—Photometry scaled assuming Sirius is $-1.36(0.07)$. Uncertainties are 1 σ from the reference and taking the Sirius scaling into account. Numbers in parentheses for DIRBE are the variability amplitudes and associated uncertainties.

0.045 mag was added to DIRBE band 1 results to correct a bias for Sirius in the DIRBE data. If a photometric reference had no Sirius measurement, Vega was then used, with magnitudes being calculated using the appropriate bandpass and the Kurucz model from Paper I. The *MSX* photometry is from Price et al. (2004), while the *IRAS* information was obtained from the VizieR Web site.[6]

The stellar effective temperature ($T_{\rm eff}$) and angular diameter (θ) in milliarcseconds were derived by fitting the *autoshape* function to the photometry. The plots show how well the *autoshape* function using the derived parameters fits the observations.

Star:

α Boo
HD 124897, HR 5340, IRAS 14133+1925
K1.5 III
CWW composite star

Fit Parameters: $T_{\rm eff} = 4350$ K, $\theta = 21.06$ mas

Spectral Data:

SWS target dedicated time (TDT): 45200101 2.4–21 μm
Hinkle et al. (1995): 2.1–2.4 μm
Strecker et al. (1979): 1.22–2.4 μm

Uncertainty:

Spectral shape: 5% near 1 μm, 3% near 2 μm, 1% for 2.5–12 μm, 1.5% beyond
Normalization relative to Sirius: 0.15%

Spectral Adjustments:

SWS: 1A $0.94(\lambda/2.5)^{0.10}$
1B $0.95(\lambda/2.6)^{0.02}$
1D $0.96(\lambda/3.0)^{0.13}$
1E $0.975(\lambda/3.7)^{0.17}$
2A $1.06(\lambda/4.05)^{0.16}$
2B $1.12(\lambda/5.35)^{0.15}$
2C $0.975(\lambda/7.4)^{0.20}$ ($7.0\ \mu{\rm m} < \lambda < 8.5\ \mu$m)
2C $1.00(\lambda/8.5)^{0.15}$ ($8.5\ \mu{\rm m} < \lambda < 10.5\ \mu$m)
2C $1.03(\lambda/10.4)^{-0.5}$ ($10.5\ \mu{\rm m} < \lambda < 11.9\ \mu$m)
2C $0.920\times$ ($\lambda \geq 11.9\ \mu$m)
3A $1.074(\lambda/12.0)^{0.1}$
3C $1.06\times$
3D $1.04(\lambda/18)^{0.15}$
Strecker et al. (1979) $0.98(\lambda/2.0)^{0.05}$
Hinkle et al. (1995) $1.005(\lambda/2.2)^{-0.35}$

[6] See http://vizier.hia.nrc.ca/viz-bin/VizieR.

REFERENCES

Alonso, A., Salaris, M., Arribas, S., Martinez-Roger, C., & Asensio Ramos, A. 2000, A&A, 355, 1060
Aringer, B., Jorgensen, U. G., & Langhoff, S. R. 1997, A&A, 323, 202
Beichman, C. A., Neugebauer, G., Habing, H. J., Clegg, P. E., & Chester, T. J., eds. 1988, *IRAS* Catalogs and Atlases: Explanatory Supplement (Washington: GPO)
Bessel, M. S., & Brett, J. M. 1988, PASP, 100, 1134
Blackwell, D. E., Lynas-Gray, A. E., & Petford, A. D. 1991, A&A, 245, 567
Blommaert, J., et al. 2003, The *ISO* Handbook, Vol. 2 (ESA SP-1262; Noordwijk: ESA)
Bouchet, P., Schmider, F. X., & Manfroid, J. 1991, A&AS, 91, 409
Bouchet, P., Slezak, E., LeBerte, T., Moneti, A., & Manfroid, J. 1989, A&AS, 80, 379
Carbon, D. F., & Gingerich, O. 1969, in Theory and Observation of Normal Stellar Atmospheres, ed. O. Gingerich (Cambridge: MIT Press), 377
Carter, B. S. 1990, MNRAS, 242, 1
———. 1993, in Precision Photometry, ed. D. Kilkenny, E. Lastovica, & J. W. Menzies (Cape Town: South African Astron. Obs.), 100
Claret, A., Diaz-Cordoves, J., & Gimenez, A. 1995, A&AS, 114, 247
Cohen, M. 1998, AJ, 115, 2092 (Paper IX)
Cohen, M., & Davies, J. K. 1995, MNRAS, 276, 715 (Paper V)
Cohen, M., Megeath, S. T., Hammersley, P. L., Martín-Luis, F., & Stauffer, J. 2003, AJ, 125, 2645 (Paper XIII)
Cohen, M., Walker, R. G., Barlow, M. J., & Deacon, J. R. 1992a, AJ, 104, 1650 (Paper I)
Cohen, M., Walker, R. G., Carter, B., Hammersley, P., & Kidger, M. 1999, AJ, 117, 1864 (Paper X)
Cohen, M., Walker, R. G., & Witteborn, F. C. 1992b, AJ, 104, 2030 (Paper II)
Cohen, M., Witteborn, F. C., Bregman, J. D., Wooden, D. H., Salama, A., & Metcalfe, L. 1996a, AJ, 112, 241 (Paper VI)
Cohen, M., Witteborn, F. C., Carbon, D. F., Davies, J. K., Wooden, D. H., & Bregman, J. D. 1996b, AJ, 112, 2274 (Paper VII)
Cohen, M., Witteborn, F. C., Walker, R. G., Bregman, J. D., & Wooden, D. H. 1995, AJ, 110, 275 (Paper IV)
Decin, L., Morris, P. W., Appleton, P. N., Charmandaris, V., Armus, L., & Houck, J. R. 2004, ApJS, 154, 408
Decin, L., Vandenbussche, B., Waelkens, C., Eriksson, K., Gustafsson, B., Plez, B., & Sauval, A. J. 2003a, A&A, 400, 709
Decin, L., Vandenbussche, B., Waelkens, C., Eriksson, K., Gustafsson, B., Plez, B., Sauval, A. J., & Hinkle, K. 2003b, A&A, 400, 679
Decin, L., Waelkens, C., Eriksson, K., Gustafsson, B., Plez, B., Sauval, A. J., Van Assche, W., & Vandenbussche, B. 2000, A&A, 364, 137
Decin, L., et al. 2003c, A&A, 400, 679
de Jager, C., & Nieuwenhuijzen, H. 1987, A&A, 177, 217
Diaz-Cordoves, J., Claret, A., & Gimenez, A. 1995, A&AS, 110, 329
Di Benedetto, G. P. 1998, A&A, 339, 858
Di Benedetto, G. P., & Bonneau, D. 1990, ApJ, 358, 617
Di Benedetto, G. P., & Rabbia, Y. 1987, A&A, 188, 114
Dreiling, L. A., & Bell, R. A. 1980, ApJ, 241, 736
Dyck, H. M., Benson, J. A., van Belle, G. T., & Ridgway, S. T. 1996, AJ, 111, 1705
Dyck, H. M., van Belle, G. T., & Thompson, R. R. 1998, AJ, 116, 981
Engelke, C. W. 1992, AJ, 104, 1248
Engelke, C. W., Kraemer, K. E., & Price, S. D. 2004, ApJS, 150, 343
Engels, D., Sherwood, W. A., Wamsteker, W., & Schultz, G. V. 1981, A&AS, 45, 5
Feast, M. W., Whitelock, P. A., & Carter, B. S. 1990, MNRAS, 247, 227
Hajian, A. R., et al. 1998, ApJ, 496, 484
Hammersley, P. L., & Jourdain de Muizon, M. 2003, in The Calibration Legacy of the *ISO* Mission, ed. L. Metcalfe et al. (ESA SP-481; Noordwijk: ESA), 129
Hammersley, P. L., Jourdain de Muizon, M., Kessler, M. F., Bouchet, P., Joseph, R. D., Habing, H. J., Salama, A., & Metcalfe, L. 1998, A&AS, 128, 207
Haniff, C. A., Scholz, M., & Tuthill, P. G. 1995, MNRAS, 276, 640
Hayes, D. L. 1985, in IAU Symp. 111, Calibration of Fundamental Stellar Quantities, ed. D. S. Hayes, E. Pasenetti, & A. G. Davis Phillip (Dordrecht: Reidel), 225
Heras, A. M., et al. 2002, A&A, 394, 539
Hinkle, K., Wallace, L., & Livingston, W. 1995, PASP, 107, 1042
Hutter, D. J., et al. 1989, ApJ, 340, 1103
Ishihara, D., et al. 2006, AJ, 131, 1074
Kenyon, S. J. 1988, AJ, 96, 337
Kerschbaum, F., & Hron, J. 1994, A&AS, 106, 397
Kervella, P., Thévenin, F., Morel, P., Bordé, P., & Di Folco, E. 2003b, A&A, 408, 681
Kervella, P., Thévenin, F., Ségrasan, D., Berthomieu, G., Lobez, B., Morel, P., & Provost, J. 2003a, A&A, 404, 1087
Kessler, M., et al. 2003, The *ISO* Handbook, Vol. 1 (ESA SP-1262; Noordwijk: ESA)
Kraemer, K. E., Sloan, G. C., Walker, H. J., & Price, S. D. 2002, ApJS, 140, 389
Leech, K., et al. 2003, The *ISO* Handbook, Vol. 5 (ESA SP-1262; Noordwijk: ESA)
Low, F. J. 1973, Ground-based Infrared Measurements (AFCRL-TR-73-0371; Cambridge: Air Force Cambridge Res. Lab.)
Manduca, A. 1979, A&AS, 36, 411
Manduca, A., Bell, R. A., & Gustafsson, B. 1981, ApJ, 243, 883
Marengo, M., Busso, M., Silvestro, G., Persi, P., & Lagage, P. O. 1999, A&A, 348, 501

Mozurkewich, D., Armstrong, J. T., Johnston, K. J., Hajian, A. R., Elias, N. M., II, Buscher, D. G., & Simon, R. S. 2003, AJ, 126, 2502
Nordgren, T. E., et al. 1999, AJ, 118, 3032
Onaka, T., et al. 2003, in The Calibration Legacy of the *ISO* Mission, ed. L. Metcalfe & M. F. K. Kessler (ESA SP-481; Noordwijk: ESA), 119
Perrin, G., Coudé du Foresto, V., Ridgway, S. T., Mariotti, J.-M., Traub, W. A., Carleton, N. P., & Lacasse, M. G. 1998, A&A, 331, 619
Pickles, A. J. 1998, PASP, 110, 863
Price, S. D. 1970, Ph.D. thesis, Ohio State Univ.
Price, S. D., Paxson, C., Engelke, C., & Murdock, T. L. 2004, AJ, 128, 889
Price, S. D., Paxson, C., Engelke, C., Murdock, T. L., & Kraemer, K. E. 2006, Air Force Res. Lab. Tech. Rep. AFRL-VS-TR-2004-1109 (Washington: GPO), in press
Quirrenbach, A., Mozurkewich, D., Buscher, D. F., Hummel, C. A., & Armstrong, J. T. 1996, A&A, 312, 160
Ramírez, I., & Meléndez, J. 2005, ApJ, 626, 446
Reach, W. T., et al. 2005, PASP, 117, 978
Richichi, A., & Roccatagliate, V. 2005, A&A, 433, 305
Ridgway, S. T., Jacoby, G. H., Joyce, R. R., Siegel, M. J., & Wells, D. C. 1982, AJ, 87, 1044
Ridgway, S. T., Joyce, R. R., White, N. M., & Wing, R. F. 1980, ApJ, 235, 126
Schild, R., Peterson, D. M., & Oke, J. B. 1971, ApJ, 166, 95
Scholz, M., & Takeda, Y. 1987, A&A, 186, 200
Selby, M. J., Hepburn, I., Blackwell, D. E., Booth, A. J., Haddock, D. J., Arribas, S., Leggett, S. K., & Mountain, C. M. 1988, A&AS, 74, 127
Sloan, G. C., Herter, T. L., Charmandaris, V., Fajardo-Acosta, S. B., Burgdorf, M., & Armus, L. 2004, BAAS, 205, 52.06
Sloan, G. C., Kraemer, K. E., Price, S. D., & Shipman, R. F. 2003, ApJS, 147, 379
Smith, B. J., Price, S. D., & Baker, R. I. 2004, ApJS, 154, 673
Strecker, D. W., Erickson, E. F., & Witteborn, F. C. 1979, ApJS, 41, 501
Strutskie, M. F., et al. 2006, AJ, 131, 1163
Thomas, J. A., Robinson, G., & Hyland, A. R. 1973, MNRAS, 165, 201
Tokunaga, A. 1984, AJ, 89, 172
Van Belle, G. T., et al. 1999, AJ, 117, 521
Van der Bliek, N. S., Manfroid, J., & Bouchet, P. 1996, A&AS, 119, 547
Vernazza, J. E., Avrett, E. H., & Loeser, R. 1976, ApJS, 30, 1
Walker, R. G., Barker, E., Cohen, M., & Jayaraman, S. 2004, Irradiance Calibration of Space-based Infrared Sensors, Final Report (AFRL-TR-2004-1161, ADA 435 636; Washington: GPO)
Walker, R. G., & Cohen, M. 1998, Infrared Celestial Background Studies, Vol. 2 [AFRL-VS-TR-98-0104(II); Washington: GPO]
———. 2002, Irradiance Calibration of Space-based Infrared Sensors, Ann. Rep. 3 (AFRL-TR-2002-1622, ADA 418 506; Washington: GPO)
Wallace, L., & Hinkle, K. 1996, ApJS, 107, 312
———. 1997, ApJS, 111, 445
Wittkowski, M., Hummel, C. A., Johnston, K. J., Mozurkewich, D., Hajian, A. R., & White, N. M. 2001, A&A, 377, 981